

FNS: an event-driven spiking neural network simulator based on the LIFL neuron model

preprint version

Gianluca Susi^{a,b}, Pilar Garcés^a, Emanuele Paracone^b, Alessandro Cristini^c,
Mario Salerno^c, Fernando Maestú^{a,d}, Ernesto Pereda^{a,1}

^aLaboratory of Cognitive and Computational Neuroscience, Center for Biomedical
Technology, Technical University of Madrid & Complutense University of Madrid, Spain.

^bDepartment of Civil Engineering and Computer Science, University of Rome ‘Tor
Vergata’, Italy

^cDepartment of Electronic Engineering, University of Rome ‘Tor Vergata’, Italy;

^dDepartment of Experimental Psychology, Cognitive Processes and Logopedy, Complutense
University of Madrid, Spain;

^eDepartment of Industrial Engineering & IUNE, University of La Laguna, Spain

Abstract

Limitations in processing capabilities and memory of today’s computers make spiking neuron-based (human) whole-brain simulations inevitably characterized by a compromise between bio-plausibility and computational cost. It translates into brain models composed of a reduced number of neurons and a simplified neuron’s mathematical model, leading to the search for new simulation strategies.

Taking advantage of the sparse character of brain-like computation, the *event-driven* technique could represent a way to carry out efficient simulation of large-scale *Spiking Neural Networks* (SNN). The recent *Leaky Integrate-and-Fire with Latency* (LIFL) spiking neuron model is event-driven compatible and exhibits some realistic neuronal features, opening new avenues for brain modelling. In this paper we introduce FNS, the first LIFL-based spiking neural network framework, which combines spiking/synaptic neural modelling

Email address: gianluca.susi@ctb.upm.es (Gianluca Susi)

with the event-driven approach, allowing us to define heterogeneous neuron modules and multi-scale connectivity with delayed connections and plastic synapses. In order to allow multi-thread implementations a novel parallelization strategy is also introduced. This paper presents mathematical models, software implementation and simulation routines on which FNS is based. Finally, a brain subnetwork is modeled on the basis of real brain structural data, and the resulting simulated activity is compared with associated brain functional (source-space MEG) data, demonstrating a good matching between the activity of the model and that of the experimental data. This work aims to lay the groundwork for future event-driven based personalised brain models.

Keywords: Spiking Neural Network, Event-driven Simulation, Neuronal modeling, Functional connectivity, Magnetoencephalography

1. Introduction

Today's advanced *magnetic resonance imaging* (MRI) -based techniques allow a thorough estimation of the structural *connectome* (i.e., the map of neural connections in the brain (Hagmann, 2005; Sporns et al., 2005)), as well as volume and morphology of single brain areas. Through the application of graph theory, such data can be employed to synthesise brain dynamic models, which today are more and more able to appropriately reproduce brain oscillations revealed by functional imaging techniques such as *Multi-Unit Activity* (MUA) and *Local Field Potential* (LFP) (Barardi et al., 2014), *functional MRI* (Cabral et al., 2011; Deco and Jirsa, 2012; Bettinardi et al., 2017) and *Magnetoencephalography* (MEG) (Nakagawa et al., 2014; Cabral et al., 2014; Deco et al., 2017), providing new information on the brain operation. In such approaches, *nodes* represent surrogates of brain regions (corresponding to *gray matter*), and *edges* represent the long-range connections, along fibre tracts, between them (corresponding to *white matter*), usually estimated using *diffusion tensor imaging* (DTI) (Fig. 1).

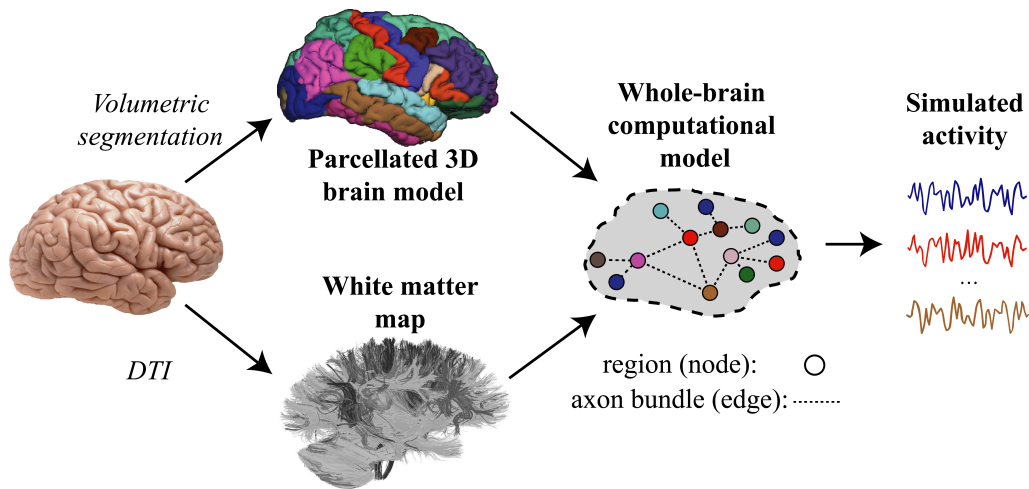


Figure 1. Synthesis of a computational brain model using the graph approach. White matter connections can be extracted by means of DTI. Brains of individual subjects can be coregistered to a parcellation template (*atlas*) in order to assign connections to specific brain areas. By assigning node local dynamics to the obtained *structural connectome*, it is possible to extract simulated activity. The number of nodes of the model depends on the template used, and each node can be represented at different levels of abstraction (e.g., ensemble of spiking neurons).

Among the different approaches used to represent brain regions (Deco et al., 2008), *spiking/synaptic models* (Vicente et al., 2008; Gollo et al., 2010; Nakagawa et al., 2014; Maslennikov and Nekorkin, 2014) present a very large number of degrees of freedom, which gives rise to highly complex and realistic behaviours on a broad frequency range of the related oscillations (Barardi et al., 2014). In addition, spiking/synaptic models offer the opportunity to relate to real-brain data transversely (*micro-*, *meso-*, and *macro-scale*, referring to the categorisation of Bohland et al., 2009), as well as to implement *spike-timing dependent plasticity* (STDP), which is indispensable in many kinds of computational neuroscience studies.

On the other hand, spiking/synaptic-based brain simulations are extremely expensive from a computational point of view (Izhikevich, 2004). This issue translates to the use of simplified spiking neuron models, and nodes composed of a low number of elements, thereby reducing the realism of the overall brain

model.

Spiking neuron models are described by differential equations and usually simulated with clock-driven (synchronous) algorithms, by means of proper integration methods (see Brette et al., 2007, for an extensive review). In this way the update is done at every tick of a clock $\mathbf{X}(t) \rightarrow \mathbf{X}(t + dt)$, and involves all network elements (neurons and possibly synapses). Such two characteristics cause a fast growth of simulation times/used memory when the network size increases, and can lead the simulation to entail missing spikes (although recent work is aimed to overcome the latter limitation, as in Hanuschkin et al. (2010) and Krishnan et al. (2017)).

Conversely, in the event-driven (or asynchronous) approach a network element is updated only when it receives or emits a spike. Then, such approach does not envisage a periodic update, neither a check of all network elements, producing simulations devoid of missed spikes, and exploits the sparseness of brain-like activity. Since the latter is irregular in time with low average (Mouraud and Puzenat, 2009), this approach has the potential to reduce the computational cost for large-scale network simulations (Ros et al., 2006). Nevertheless, the need of an explicit solution for the neuron state between spikes, and the consideration of incoming and outgoing pulses as discrete events, make the event-driven simulation of classic bio-realistic models very challenging. This has stimulated a big interest in scientific community in developing both realistic and event-driven-compatible spiking neuron models (see Brette, 2006, 2007; Tonnelier et al., 2007; Salerno et al., 2011; Rudolph-Lilith et al., 2012), which led to the development of event-driven based SNN simulators (see Pecevski et al., 2014; Cristini et al., 2015), and hybrid *event/time-step* based simulation strategies (see Morrison et al., 2006; Hanuschkin et al., 2010; D’Haene et al., 2014; Gewaltig and Diesmann, 2007; Brette and Goodman, 2016).

In particular, the *Leaky Integrate-and-Fire with Latency* (LIFL) model is a recent neuron model that can be simulated in event-driven fashion, preserving

important computational features at the same time (Susi et al., 2018a; Salerno et al., 2011; Cardarilli et al., 2013; Cristini et al., 2015; Susi, 2015; Susi et al., 2016; Acciarito et al., 2017). Differently from the *Leaky Integrate-and-Fire* (LIF), LIFL incorporates important neuronal features extracted from the bio-realistic *Hodgkin-Huxley* (HH) model, such as the *spike latency* (FitzHugh, 1955; Izhikevich, 2004). The latter has been proved to be fundamental in many scenarios of neural computation, providing a large range of behaviors. Then, the LIFL may open new avenues for the efficient simulation of large scale brain models.

In this work we present FNS (literally, *Firnet NeuroScience*), a LIFL-based exact event-driven SNN framework oriented to brain simulations, implemented in *Java*. FNS allows us to generate brain network models on the basis of a versatile graph-based multi-scale neuroanatomical connectivity scheme, allowing for heterogeneous neuron modules and connections. In addition to the high-customizability of the network, proper input and output sections make it possible to relate model activity to real data, with the option to enable plasticity, then making the network parameters evolve depending on the network activity.

In section 2, we describe the neurobiological principles and mathematical models on which FNS is based: neuron model, region model, fibre tracts model, plasticity, input and output signals.

In section 3, we present the possibilities that the framework offers for the synthesis of custom models and the design of specific simulations: generator section, neuroanatomical model section and output section.

In section 4, we illustrate the technical aspects of the simulation framework itself: design principles, data structures and parallelization strategy.

In section 5, we present an example to show how to conduct a simulation in FNS, and to evaluate the realism and performances of the framework itself. In short, we model a brain subnetwork using structural data of a real subject, and through FNS we simulate brain activity and synthesize

electrophysiological-like output signals. Then, we compare such signals with those of the real subject.

In the Discussion section, we summarize our work and envisage how to improve FNS in future works.

In this manuscript, a single neuron is indicated with n ; an axonal connection between two whichever neurons with e ; a neuron module (corresponding to a region or subregion in real case) with N , and called *network node*; the complete set of connections between two nodes (corresponding to fibre tracts in real case) with E , and called *network edge*.

The software can be freely downloaded at:
www.fnsneuralsimulator.org.

In the download link a user guide (including a short description of how to install and run it) and some network models are also provided with the software.

2. From neurobiology to mathematical models

Specificity and heterogeneity characterize the human brain at all scales. In this regard, recent works highlight crucial aspects that have to be taken into account in brain models to obtain realistic dynamics:

- *Region bioplausibility*: in spiking/synaptic models, an inappropriate choice of the spiking neuron model or the intra-module connectivity configuration may lead to results having nothing to do with the information processing of real brain (Izhikevich, 2004). Of course, also the cardinality of the nodes is important for achieving an appropriate network behaviour.
- *Region diversity*: diversity among and within regions specializes the behaviour of single parts of the network, enhancing the information content and coding performances and shaping properties of collective

behavior such as synchronization (see Thivierge, 2008; Gollo et al., 2016).

- *Inter-region connection bioplausibility*: synchronization between network nodes is strongly sensitive to edge parameters (as weights, delays and connection number) and their distributions (Brunel and Hakim, 1999; Brunel and Wang, 2003; Vicente et al., 2008; Viriyopase et al., 2012; Gollo et al., 2014).
- *Inter-region connection diversity*: selective variations of edge parameters are able to reconfigure the network synchronization profile (Abuhassan et al., 2014), including synchronization between nodes that are not directly connected to the modified edge Gollo et al. (2014).

FNS aims to guarantee the possibility to take into account such aspects in order to avoid the alteration of the network operation. In this section we present mathematical models used in FNS.

2.1. LIFL Neuron model

Although the classic LIF model is very fast to simulate, it has been regarded as unrealistically simple, thereby incapable of reproducing the dynamics exhibited by cortical neurons (Izhikevich, 2003). FNS is based on the LIFL, that besides being computationally simple it is also able to support a greater number of neuronal features than the LIF.

2.1.1. A brief introduction to the spike latency neuro-computational feature

The *spike latency* is the membrane potential-dependent delay time between the overcoming of the “threshold” potential and the actual spike generation (Izhikevich, 2004). Among all the neuron features, it is of considerable importance because it extends the neuron computation capabilities over the “threshold”, giving rise to a range of new behaviors. Spike latency is ubiquitous in the nervous system, including the auditory, visual, and somatosensory systems (Wang et al., 2013; Trotta et al., 2013).

From a computational point of view it provides a spike-timing mechanism to encode the strength of the input (Izhikevich, 2007) conferring many coding/decoding capabilities to the network (e.g., Gollisch and Meister, 2008; Fontaine and Peremans, 2009; Susi, 2015), whereas, from a statistical point of view it results in a desynchronizing effect (Salerno et al., 2011; Cardarilli et al., 2013), fostering the emergence of higher frequencies (Susi et al., 2016) and providing robustness to noise to the network (Izhikevich, 2007, chapter 7). Spike latency has already been introduced in some variants of the LIF, as *QIF* (Vilela and Lindner, 2009) and *EIF* (Fourcaud-Trocme et al., 2003). In LIFL spike latency is embedded with a mechanism extracted from the realistic HH model (Salerno et al., 2011), both simple and suitable to the event-driven simulation strategy.

2.1.2. LIFL operation

In this section, we briefly describe the behaviour of the LIFL neuron model. For the sake of simplicity, we will refer to its basic configuration.

LIFL neuron model is characterized by a real non-negative quantity S (the *inner state*, corresponding to the membrane potential of the biological neuron), which is defined from 0 (corresponding to the resting potential of the biological neuron) to S_{max} (*maximum state*), a value much greater than one, at most ∞ . Simple Dirac delta functions (representing the action potentials) are supposed to be exchanged between network's neurons, in form of *pulse* trains. The model is able to operate in two different modes: *passive mode* when $S < S_{th}$, and *active mode* when $S \geq S_{th}$, where S_{th} is the *firing threshold*, a value slightly greater than 1. In passive mode, S is affected by a decay, whereas the active mode is characterized by a spontaneous growth of S . Assuming that neuron n_j (i.e., the *post-synaptic neuron*) is receiving a pulse from neuron n_i (i.e., the *pre-synaptic neuron*), its inner state is updated through one of the following equations, depending on whether n_j was in passive or in active mode, respectively:

$$S_j = \begin{cases} S_{p_j} + A_i \cdot W_{i,j} - T_l, & \text{for } 0 \leq S_{p_j} < S_{th} & (1a) \\ S_{p_j} + A_i \cdot W_{i,j} + T_r, & \text{for } S_{th} \leq S_{p_j} < S_{max} & (1b) \end{cases}$$

S_{p_j} represents the post-synaptic neuron's *previous state*, i.e., the inner state immediately before the new pulse arrives. A_i represents the *pre-synaptic amplitude*, which is related to the pre-synaptic neuron, and can be positive or negative depending on whether the neuron sends excitatory or inhibitory connections, respectively.

$W_{i,j}$ represents the *post-synaptic weight* related to the pre-/post-synaptic neuron couple; if this quantity is equal to 0, the related connection is not present. The product $A_i \cdot W_{i,j}$ globally represents the amplitude of the pulse arriving to the post-synaptic neuron n_j (i.e., the *synaptic pulse*) from the pre-synaptic neuron n_i . In this paper, w or ω will be used instead of W , depending on the connection is intra- or inter- node, respectively.

T_l (the *leakage term*) takes into account the behaviour of S during two consecutive input pulses in passive mode. The user is allowed to select among two kinds of underthreshold decay: *linear* decay (as in Mattia and Del Giudice, 2000) or *exponential* decay (as in Barranca et al., 2014), which behaviour is modulated by the *decay parameter* D , as explained in the *Appendix A*.

T_r (the *rise term*) takes into account the overthreshold growth acting upon S during two consecutive input pulses in active mode. Specifically, once the neuron's inner state crosses the threshold, the neuron is ready to fire. The firing is not instantaneous, but it occurs after a continuous-time delay, representing the spike latency, that we call *time-to-fire* and indicate with t_f in our model. This quantity can be affected by further inputs, making the neuron sensitive to changes in the network spiking activity for a certain time window, until the actual spike generation. S and t_f are related through the

following bijective relationship, called the *firing equation*:

$$t_f = \frac{a}{(S - 1)} - b \quad (2)$$

where $a, b \geq 0$. Such rectangular hyperbola has been obtained through the simulation of a membrane patch stimulated by brief current pulses (i.e., 0.01 *ms* of duration), solving the Hodgkin-Huxley equations (Hodgkin and Huxley, 1952) in *NEURON* environment (Hines and Carnevale, 1997), as described in Salerno et al. (2011). Then, if the inner state of a neuron is known, the related t_f can be exactly calculated by means of Eq. 2. As introduced in 2.1.1, this nonlinear trend has been observed in most cortical neurons (Izhikevich, 2004); similar behaviors have been also found by other authors, such as Wang et al. (2013) and Trotta et al. (2013), using DC inputs. Conversely to previous versions of LIFL (Cristini et al., 2015; Susi et al., 2018a), positive constants a and b have been introduced in order to make the model able to encompass the latency curves of a greater number of neuron types; in particular, a allows us to distance/approach the hyperbola to its centre, while b allows us to define a S_{max} , conferring a bio-physical meaning to the inner state in active mode (note that if $b = 0$, then $S_{max} = \infty$; nevertheless, the neuron will continue to show the spike latency feature).

The firing threshold can be equivalently written as:

$$S_{th} = 1 + c \quad (3)$$

where c is a positive value called *threshold constant*, that fixes a bound for the maximum t_f . According to Eq. 3, when $S = S_{th}$, the t_f is maximum, and equal to:

$$t_{f,max} = a/c - b \quad (4)$$

where $t_{f,max}$ represents the upper bound of the time-to-fire. As mentioned above, the latter consideration is crucial in order to have a finite maximum

spike latency as in biological neurons (FitzHugh, 1955). From the last equation, we obtain the restriction $c < a/b$.

As described in *Appendix B*, using Eq. 2, it is possible to obtain T_r (*rise term*), as follows:

$$T_r = \frac{(S_p - 1)^2 \Delta t}{a - (S_p - 1) \Delta t} \quad (5)$$

in which S_p represents the previous state, whereas Δt is the temporal distance between two consecutive incoming pre-synaptic spikes. The Eq. 5 allows us to determine the inner state of a neuron at the time that it receives further inputs during the t_f time window. In Fig. 2, the operation of LIFL is illustrated, while the effect of Eq. 5 is shown in Fig. 3.

Assuming that an input spike leads the inner state overthreshold at time t_A , the arrival of a contribution during the latency time (i.e., at time t_B) results in a new t_f (i.e., a change of the firing time). Excitatory (inhibitory) inputs increase (decrease) the inner state of a post-synaptic neuron. Therefore, when a neuron is in active mode, excitatory (inhibitory) inputs decrease (increase) the related time-to-fire (*post-trigger anticipation/postponement* respectively). If the inhibitory effect is as strong as to pull the post-synaptic neuron state under the firing threshold, its t_f will be suppressed and its state will come back to the passive mode (*post-trigger inhibition*) (Salerno et al., 2011; Cristini et al., 2015).

For a given neuron j in active mode, the arrival of new input contributions provokes t_f updating. Once the t_f is reached, the output spike is generated and the inner state is reset. Note that if incoming spikes are such as to bring S to a value < 0 ($> S_{max}$), S is automatically put to 0 (a spike is immediately generated). We emphasize the fact that spike latency enables a mechanism to encode neural information, supported from all the most plausible models. Thus, there is lack of information in models that do not exhibit this relevant property.

Hitherto we have discussed a basic configuration of LIFL, which defines

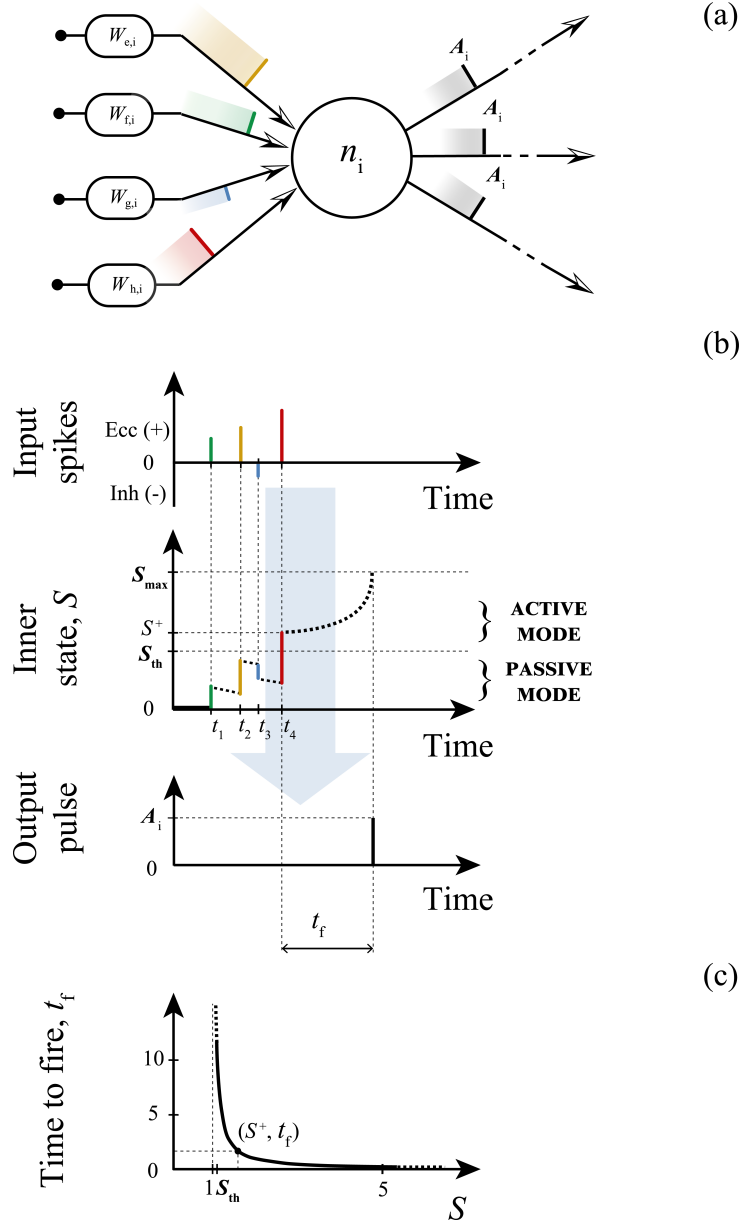


Figure 2. Neural summation and spike generation in a LIFL neuron. (a) Input/output process scheme; (b) temporal diagram of LIFL operation (basic configuration), assuming the neuron starts from its resting potential. Each incoming excitatory (inhibitory) input causes an instantaneous increase (decrease) of the inner state. In passive mode the neuron is affected by a decay; when S exceeds the threshold ($S = S^+$) the neuron is ready to spike; due to the latency effect, the firing is not instantaneous but it occurs after t_f . Once emitted, the pulse of amplitude A_i (positive, if the neuron i is excitatory as supposed to be in this case, without loss of generality) is routed to all the subsequent connections. In (c) is shown the firing equation, i.e., the latency curve for the determination of t_f from S^+ (see Salerno et al., 2011). The simplest case of firing equation curve has been chosen ($a = 1$, $b = 0$), and c set to 0.04

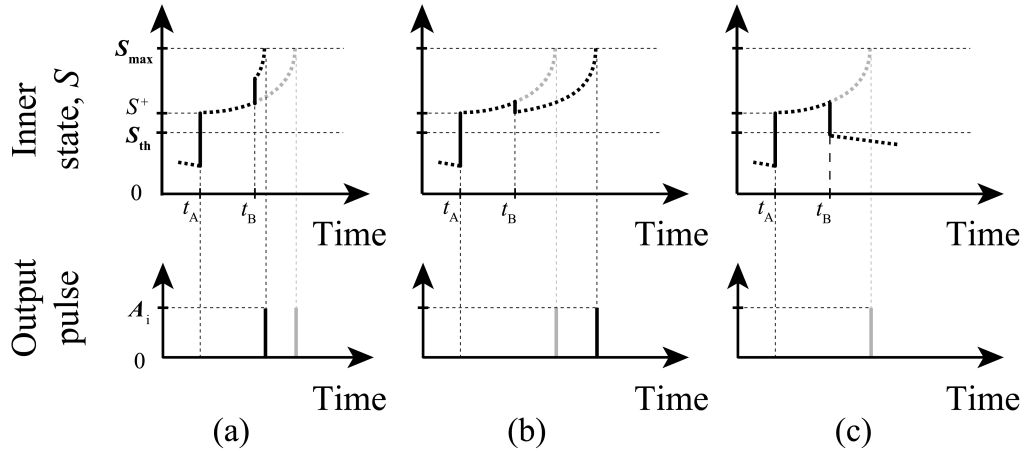


Figure 3. Arrival of further inputs when the neuron is overthreshold. (a) The arrival of a new excitatory synaptic pulse at time t_B anticipates the spike generation (post-trigger anticipation). The arrival of a new inhibitory synaptic pulse at time t_B is able to (b) delay the spike generation (post-trigger postponement), or (c) to cancel the spike generation (post-trigger inhibition). In order to simplify the comparison, the state evolution in active mode in the simple case of no further inputs is reported in the same figure (grey). Neuron i is supposed to be excitatory as in Fig. 2.

an intrinsically *class 1 excitable, integrator* neuron, supporting *tonic spiking* and *spike latency*. Nevertheless, thanks to the simplicity of its mathematical model, it can be easily enriched with other neuro-computational features to reproduce different kinds of cortical neurons (see Izhikevich, 2004) by introducing minimal modifications to the model equations, or by adding extrinsic properties at the programming level. This is the case of *refractory period* for which the neuron becomes insensitive, for a period t_{arp} , to further incoming spikes after the spike generation, and *tonic bursting* for which the neuron produces a train of N_b spikes interspaced by an interval *IBI*, instead of a single one.

In addition to the spike latency, emerging from the pure computation of the neuron, in the next section another kind of delay will be introduced, independent from the activity, used to characterize the long-range connections between neurons belonging to different groups.

2.2. Connection between 2 neurons

In FNS the network nodes are composed of modules of spiking neurons to represent brain regions. Neurons of the same node interact instantaneously, whereas a settable time delay (≥ 0) is present between neurons of different nodes to reflect the remoteness between the regions to which they pertain.

A scheme of inter-node neuron connection ($e_{i,j}$) is illustrated in Fig. 4, where $\lambda_{i,j}$ represents the *axonal length* block and $\omega_{i,j}$ represents the *post-synaptic weight* block. Such two link elements (belonging to a directed connection) are able to introduce delay and amplification/attenuation of the passing pulse, respectively. As in Nakagawa et al. (2014); Cabral et al. (2014) a global propagation speed v is set for FNS simulations, so that inter-node connection delays are automatically defined from the axonal lengths, as $\tau_{i,j} = \lambda_{i,j}/v$. Connection delays are important since they allow to take into account the three-dimensionality (i.e., spatial embeddedness) of the real anatomical brain networks. For the motivations mentioned before, conversely to the inter-node connection (represented as $e_{i,j}$ in Fig. 5), intra-node connection (represented as $e_{j,k}$ in the same Figure) does not provide the axonal length block (although synaptic weight block continues to be defined).

For biological and mathematical reasons, it is desirable to keep the synaptic weights under a certain value, W_{max} , a global parameter of the model.

In the following sections we call *firing event* the pulse emission by a pre-synaptic neuron, and *burning event* the pulse delivery to a post-synaptic neuron.

2.3. From brain regions to graph nodes

FNS allows us to define regions constituted by one or more *nodes* where each node consists of a neuron module with specific properties. In order to reproduce heterogeneous nodes, a Watts-Strogatz based generative procedure is implemented (Watts and Strogatz, 1998) as detailed below, allowing the generation of complex networks with structure properties of real neuron populations.

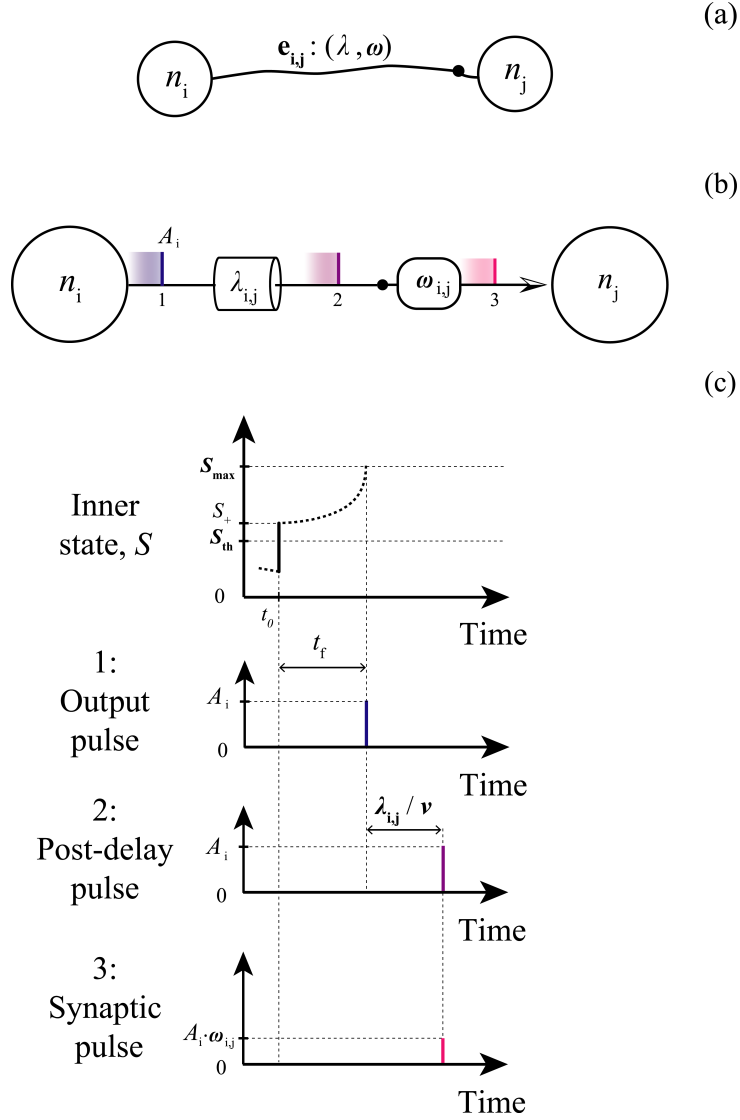


Figure 4. Neuron connection model and pulse transfer. (a) compact representation, (b) logical block representation, (c) temporal diagram: length block produces a translation of the output pulse along time axis. Note that in this example the neuron is supposed to be excitatory, otherwise all the amplitudes would be negative. Output pulses can be considered as a correlate of spiking activity, whereas synaptic pulses can be considered as correlate of synaptic currents. Note that in a) and b) the black dot represents the synaptic junction

The implemented procedure allows us to model intra- and inter-node diversity: number of neurons and connectivity, percentage of inhibitory neurons, distribution of weights and type of neuron; in addition, it is possible to represent a region with more than one node to model intra-region neuronal pools of different connectivity and neuron types. In the extreme case, a module can be composed of a single neuron, e.g., for reproducing small and deterministic motifs. In the following sections we illustrate the procedure used by FNS for the generation of network nodes and the structure of intra- and inter- node connections.

2.3.1. Watts-Strogatz-based module generation procedure

The original Watts-Strogatz procedure is able to generate different types of complex networks (from regular to random), including networks with *small-world* properties (i.e., networks that present large *clustering coefficient* and small *average path length*), that has been demonstrated to reasonably approximate a mid-sized patch of cortex (in the order of $10\mu m$) with its neighborhood (Riecke et al., 2007). The original Watts-Strogatz procedure is here adapted to generate a module including both inhibitory and excitatory, oriented, connections, analogously to Maslennikov and Nekorkin (2014). Given the integer n (i.e., *number of neurons*), k (i.e., *mean degree*), p (i.e., *rewiring probability*), and R (i.e., *excitatory ratio*), with $0 \leq p \leq 1$ and $n \gg k \gg \ln(n) \gg 1$, the model generates an oriented graph with n vertices and nk single connections in the following way:

- a regular ring lattice of n spiking neurons is created, of which $R \cdot n$ are able to send excitatory connections and the remaining $(1 - R) \cdot n$ are able to send inhibitory connections;
- for each neuron an outgoing connection to the closest k neurons is generated ($k/2$ connections for each side, with k integer and even);
- for each neuron i , every link $e_{i,j}$ with $i < j$, is rewired with probability p ; rewiring is done by exchanging $e_{i,j}$ and $e_{i,m}$ where m is chosen with

uniform probability from all possible (excitatory or inhibitory) neurons that avoid self-loops ($m \neq i$) and link duplication. This process is repeated n times, each one considering a different neuron.

Note that the p parameter allows to interpolate between a regular lattice ($p = 0$) and a random graph ($p = 1$): as p increases, the graph becomes increasingly disordered. For intermediate values of p the network presents small-world properties. The parameters n, k, p allow the user to customize the network nodes on the basis of the real anatomy. For example, n can be chosen in accord to the volume of the region that is intended to be represented (estimated from a specific subject through volumetry, or extracted from existing *atlases*).

2.3.2. Characterization of intra-module connections

Once connections have been established, weights have to be assigned. Several authors have addressed this problem, setting intra-node weights in different manners. Depending on the specific study, weights have been chosen to have the same, static value (Deco and Jirsa, 2012), or characterized by a specific distribution (Abuhassan et al., 2014), or varying in a certain range by means of plasticity (Izhikevich et al., 2004). In order to encompass the most of these possibilities, in FNS a set of Gaussian distributed values can be defined by the user for the initialization of the intra-module post-synaptic weights of each module.

2.4. From fibre tracts to graph edges

In FSN an *edge* represents a monodirectional set of long-range axons that links a module to another. In the brain, inter-region connections are often characterized by non negligible delays, which are determined by axon length, diameter and myelination.

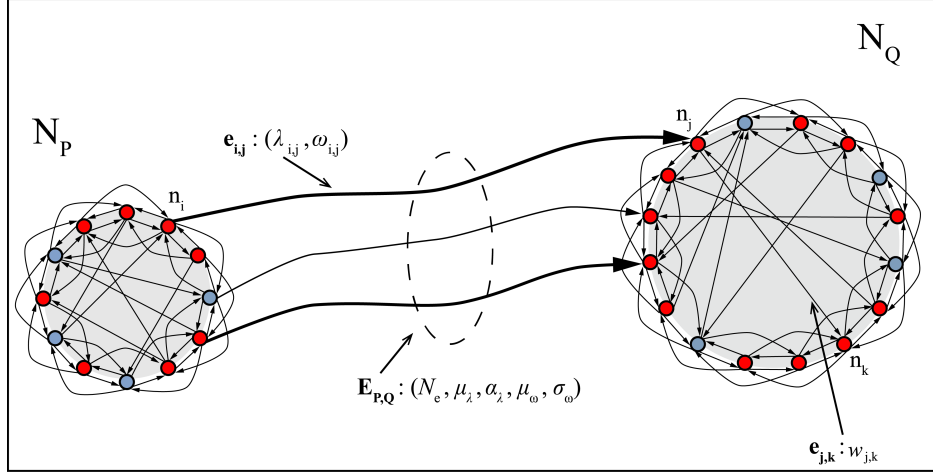


Figure 5. Two nodes connected by an edge. While an intra-node connection is characterized by its weight, an inter-node connection is defined by weight and length; an edge is defined by number of axons and related distribution of weights and lengths. In order to represent the two modules, for illustrative purpose the following values are used: $n_1 = 12$, $n_2 = 16$; $R_1 = 2/3$, $R_2 = 3/4$; $k_1 = k_2 = 4$; $p_1 = 1/6$, $p_2 = 1/8$.

2.4.1. Characterization of inter-region connections

FNS allows the user to set proper number of connections N_e and distributions of weights and lengths can for the network edges. The distribution of edge weights follows a Gaussian function (as in Abuhassan et al., 2014), characterized by the parameters μ_ω and σ_ω . Differently, a gamma distribution is implemented for the edge lengths, characterized by mean parameter μ_λ and shape parameter α_λ (see *Appendix C*), since there is probably not a unique prototypical shape for edge delays (as discussed in Vicente et al., 2008). Indeed, this distribution allows the user to explore different shapes, to investigate the impact of different choices on the network activity, to mimic pathological states as the effect of structural inhomogeneity (as discussed in Ton et al., 2014), or spatially-selective conduction speed decrease due to demyelination (Smith, 1994).

When defining inter-region edges, the user can specify the kind of connections to set among the nodes (excitatory, inhibitory, mixed).

2.5. STDP

Synaptic plasticity consists of an unsupervised spike-based process able to modify weights on the basis of the network activity. The STDP, a well-known type of plasticity mechanism, is believed to underlie learning and information storage in the brain, and refine neuronal circuits during brain development (Sjöström and Gerstner, 2010). Considering a synapse connecting two neurons, such mechanism is based on the precise timings of *pre-synaptic pulse* (i.e., the *synaptic pulse* arriving from the pre-synaptic neuron) and *post-synaptic pulse* (i.e., the *output pulse* generated by the post-synaptic neuron), influencing the magnitude and direction of change of the synaptic weight. In case of inter-node connection the pre-synaptic pulse is taken after the axonal delay block and not before, in order to not to alter information on causality between pulse arrival and pulse generation. The original STDP behaviour Bi and Poo (1998) can be approximated by two exponential functions (Abbott and Nelson, 2000).

$$\Delta W = \begin{cases} A_+ e^{-\frac{\Delta T}{\tau_+}}, & \text{for } \Delta T > 0 & (6a) \\ 0, & \text{for } \Delta T = 0 & (6b) \\ A_- e^{\frac{\Delta T}{\tau_-}}, & \text{for } \Delta T < 0 & (6c) \end{cases}$$

where:

- ΔT is the difference between post-synaptic pulse generation (i.e., t_{post}) and pre-synaptic pulse arrival (i.e., t_{pre}) instants:

$$\Delta T = t_{post} - t_{pre} \quad (7)$$

as illustrated in Fig. 6

- τ_+ and τ_- are positive time constants for *long-term potentiation* (LTP, 6a) and *long-term depression* (LTD, 6c), respectively;

- A_+ and A_- are chosen in order to keep weight values bounded between minimum and maximum values (as discussed in Sect. 2.2).

Then, weight is increased or decreased depending on the pulse order (*pre*-before *post*-, or *post*- before *pre*-, respectively). To make the weight change dependent also on the current weight value, *soft bounds* (Sjöström and Gerstner, 2010) are introduced in FNS, so that $A_+(W_p) = (W_{max} - W_p)\eta_+$ and $A_-(W_p) = W_p\eta_-$, where W_p is the past value of the synaptic weight, W_{max} the upper bound (see 2.2), and η_+ and η_- are positive learning constants, usually in the order of $\sim 10^{-5}$. Therefore, the weight update relations implemented in FNS are:

$$W = \begin{cases} W_p + (W_{max} - W_p)\eta_+ e^{-\frac{\Delta T}{\tau_+}}, & \text{for } \Delta T \geq 0 \\ W_p - W_p\eta_- e^{\frac{\Delta T}{\tau_-}}, & \text{for } \Delta T < 0 \end{cases} \quad (8a)$$

$$(8b)$$

It is important to stress that the *soft-bounds* approach allows an increase of both the synaptic capacity and the memory lifetime, with respect to the alternative *hard-bounds* approach (van Rossum et al., 2012).

In addition, to simplify the STDP event list management, exponential tails are suppressed after a certain time value $TO \cdot \max(\tau_+, \tau_-)$, where TO is the *STDP timeout constant*, defined by the user, and usually in the order of 100 ms. In this way, neuron couples whose interval exceeds such time limit are not considered for the STDP process (see Fig. 6).

STDP varies tremendously across synapse types and brain regions (Abbott and Nelson, 2000; Caporale and Dan, 2008). Accordingly, in FNS it is possible to specify a different set of STDP parameters for each node, or to apply STDP uniquely for certain nodes.

2.6. Input stimuli

Several types of stimuli can be of interest in brain simulation studies. Of these, two prototypical types of stimuli are:

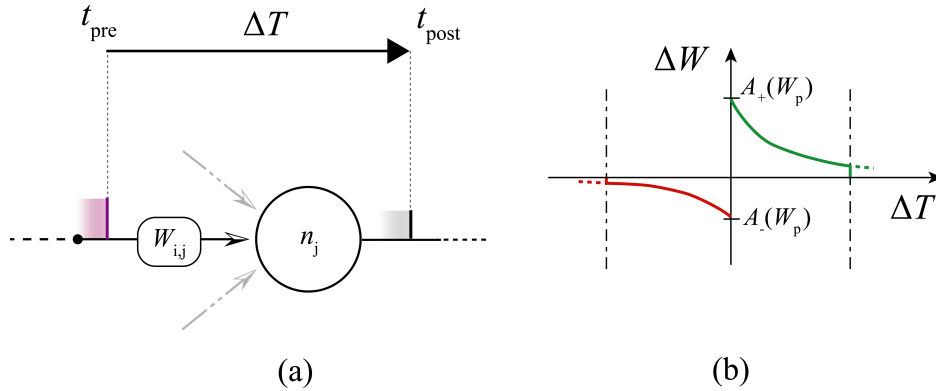


Figure 6. STDP process in FNS: (a) ΔT calculation in relation to the synapse w_{ij} , considering an inter-module connection (without loss of generality); (b) Shapes of the learning windows (LTP in green, LTD in red) considering exponential tail suppression (dash dot).

- the noisy fluctuations typically observed in vivo, which can be modeled by uncorrelated Poisson-distributed spike trains (see Frohlich et al., 2008; Abuhassan et al., 2014; Nakagawa et al., 2014);
- the DC current used by neurophysiologists to test some neuron features (Izhikevich, 2004) that can be modeled by constant spike trains (as in Vicente et al., 2008).

In addition, in many simulation scenarios the possibility of giving arbitrary spike streams (e.g., sequences that mimic sensory-like processed data) can be of interest, in order to test the response of specific subnetworks.

In light of these observations, in FNS it is possible to stimulate brain nodes with three different types of inputs: *Poisson-distributed spike train*, *constant spike train*, and *arbitrary spike stream*. The user is allowed to stimulate all or only a part of the network nodes, choosing for each kind of input a customizable number of fictive excitatory *external neurons*, and the characteristics of the required stimuli.

2.6.1. Poisson-distributed spike train

This option provides the injection of spike trains distributed according to an homogeneous Poisson process, in which the underlying *instantaneous firing rate* r_P (Gerstner et al., 2014), is constant over time.

Given a long interval (t_A, t_B) we place a single spike in that interval at random. Then, considering the sub-interval (t_1, t_2) of length $\Delta t = t_2 - t_1$, the probability that the spike occurs during this sub-interval is equal to $\Delta t / (t_B - t_A)$. Now, placing k spikes in the long interval, the probability that n of them fall in the sub-interval is given by the following binomial formula:

$$P\{n \text{ spikes during } \Delta t\} = \frac{k!}{(k-n)!n!} p^n q^{k-n} \quad (9)$$

where $p = \delta t / (t_B - t_A)$ and $q = 1 - p$.

Under proper conditions this expression can be rewritten removing the time dependence as:

$$P\{1 \text{ spike during } \delta t\} \approx r \delta t \quad (10)$$

This equation can be used to generate a Poisson spike train by first subdividing time into a set of short intervals, each one of duration δt . Then generate a sequence of random numbers \mathbf{R} , uniformly distributed between 0 and 1. For each interval i , a spike is generated if $\mathbf{R}(i) \leq r \delta t$. This procedure is appropriate only when δt is very small, i.e, only when $r \delta t \ll 1$ (Heeger and Heeger, 2000).

In FNS, a user-defined number of fictive *external neurons* $n_{extP,k}$ is set for each stimulated node N_k . By defining a $t_{startP,k}$ and a $t_{endP,k}$ for the external stimuli, each external neuron can send spikes in a discrete number of instants $(t_{startP,k} - t_{endP,k}) / \delta t_P$. The target neurons receive pulses of amplitude $A_{P,k}$.

Pulses are injected from each external neuron to all neurons belonging to a set of nodes defined by the user, by specifying the following set of parameters

for each chosen node N_k : $n_{extP,k}$, $t_{startP,k}$, $t_{endP,k}$, $r_{P,k}$, $\delta t_{P,k}$ and $A_{P,k}$.

2.6.2. Constant spike train

This option provides the injection of constant spike trains in order to emulate DC current stimulation. Note that since we simulate the network by means of an event-driven approach, the *DC* input is not continuous as in the real counterpart, but it is constantly sampled with an adequately small time step (i.e., smaller than the spike duration) called *interspike interval* and indicated with int_c .

In FNS, a user-defined number of fictive *external neurons* $n_{extc,k}$ is set for each stimulated node N_k . Each external neuron can send spikes from time $t_{startc,k}$ to $t_{endc,k}$, with amplitude $A_{c,k}$. Such kind of input is injected from each external neuron to all neurons belonging to a set of nodes defined by the user, by specifying the following set of parameters for each chosen node N_k : $n_{extc,k}$, $t_{startc,k}$, $t_{endc,k}$, $int_{c,k}$ and $A_{c,k}$.

Note that the situation $int_{c,k} < t_{arp,k}$ should be avoided because pulses would arrive during the refractory time.

2.6.3. Arbitrary spike stream

Arbitrary spike streams can be injected to neurons belonging to a set of nodes defined by the user by specifying the following set of parameters for each chosen node N_k : the spike *amplitude* $A_{ss,k}$, and a couple $(n_{ss,k}, t_{ss,k})$ for each event to introduce (i.e., *external source number* and related *spike timing*, respectively). External sources are permanently associated to the neurons of the indicated node, using a random procedure.

2.7. Output signals

Depending on the type of contributions we are considering at the network level, i.e., output pulses (corresponding to *action potentials*) or synaptic pulses (corresponding to *post-synaptic currents*), the same network activity gives rise to different signals, due to the presence of connection delays and weights.

In particular, action potentials coincide with the activity emerging from *firing* events (see Sect. 2.1.2), because they take place before the axon, thus they are spatially localized at the emitter node; whereas post-synaptic currents coincide with the post-synaptic activity (see Sect. 2.1.2), because they take place downstream the axon, thus they are spatially localized to the receiver node, and are affected by the shifting effect introduced by (heterogeneous) fibre tract’s delays and post-synaptic weights.

Action potentials are of interest for some studies (see Vicente et al., 2008), whereas post-synaptic currents can be useful for some others (see Mazzoni et al. (2008); Nakagawa et al. (2014) for LFP and MEG signal reconstruction).

In order to give the user the possibility to reconstruct such different types of signals, output section of FNS allows to store both pulse emission and arrival times (t_F and t_B), transmitter and receiver neurons (n_F and n_B) and related nodes (N_F and N_B), as well as amplitude weights (W_{ev}) involved in each event occurring during the simulation interval, for some nodes indicated by the user before the simulation starts.

3. Simulation framework structure

On the basis of the modelling introduced in the previous section, here we describe the framework structure and the tools it offers to the user for implementing a custom network, stimulating it, and obtaining the outputs of interest.

The framework is articulated in three main sections : *Generator section*, *Neuroanatomical model section* and *Output section* (see Fig. 7). In order to design a simulation, the user interacts with such sections by means of proper configuration files, that are internally translated into configuration *vectors*, which are defined in table 1.

Section	Vector	Components	Name
Generator section	PV	n_{extP}	number of <i>Poisson spike train</i> external neurons
		t_{startP}	Poisson input onset
		t_{endP}	Poisson input offset
		r_P	firing rate
		δt_P	delta
		A_P	Poisson input amplitude
	CV	n_{extc}	number of <i>constant spike train</i> external neurons
		t_{startc}	constant input onset
		t_{endc}	constant input offset
		int_c	interspike interval
		A_c	constant input amplitude
	SV	t_{ss1}, t_{ss2}, \dots	<i>input stream</i> spike timings
		n_{ss1}, n_{ss2}, \dots	related neuron numbers
		A_{ss}	stream input amplitude
	Neuroanatomical module section	LDV	n
p			rewiring probability
k			mean degree
R			excitatory ratio
A_{exc}			excitatory pre-synaptic amplitude
A_{inh}			inhibitory pre-synaptic amplitude
μ_w			intra-node post-synaptic weight distr.mean (Gaussian)
σ_w			intra-node post-synaptic weight distr.st.dev. (Gaussian)
a			latency curve center distance
b			latency curve x-axis intersection
c			threshold constant
D			decay parameter
t_{arp}			absolute refractory period
N_b			burst number
IBI			inter-burst interval
ICV		N_e	number of connections (edge cardinality)
		μ_ω	inter-node post-synaptic weight distr.mean (Gaussian)
		σ_ω	inter-node post-synaptic weight distr.st.dev. (Gaussian)
		μ_λ	inter-node length distr.mean (gamma)
		α_λ	inter-node length distr.shape (gamma)
STDPV		τ_+	LTP time constant
		τ_-	LTD time constant
		η_+	LTP learning constant
		η_-	LTD learning constant
		TO	STDP timeout constant
GPV		W_{max}	maximum weight
		v	global conduction speed
	t_{stop}	simulation stop time	
Output section	NV	NOI_1, NOI_2, \dots	list of <i>NOIs</i>
	FV	n_F	pre-synaptic neuron number (if firing event)

		N_F	pre-synaptic node number (if firing event)
		t_F	firing event time (if firing event)
	BV	n_B	post-synaptic neuron number (if burning event)
		N_B	post-synaptic node number (if burning event)
		t_B	pulse arrival time (if burning event)
		W_B	synaptic weight (if burning event)

Table 1. Definition of the system parameters.

3.1. Generator section

This section allows the user to inject the desired input to some selected nodes. *Poisson spike train vectors* (i.e., **PV**), *constant spike train vectors* (i.e., **CV**) and *arbitrary spike stream vectors* (i.e., **SV**) can be combined to send more than a kind of input to the same node simultaneously.

3.2. Neuroanatomical model section

This section allows the user to define the network model: local dynamics, structural parameters, plasticity constants and global parameters. Each node is fully characterized by a *local dynamics vector* (i.e., **LDV**), consisting of *local topology parameters*, *intra-node connection parameters* and *neuron parameters*. From the definition of node’s weight distribution, the simulator computes all the single intra-node synaptic weights and stores them in proper data structures (see Sect. 4.1).

Each edge is fully characterized by a *inter-connectivity vector* (i.e., **ICV**), consisting of *edge cardinality* and *inter-node weight distribution* and *length distribution parameters*. From the definition of such parameters the simulator computes all the single inter-node lengths and weights and stores them in proper data structures (see Sect. 4.1).

Note that values arising from the distribution of inter-node lengths have to be positive to be stored in the internal matrices; in case they assume negative values FNS allows the user to consider the absolute value of such quantities, or to terminate the program execution. In addition, weight values are kept

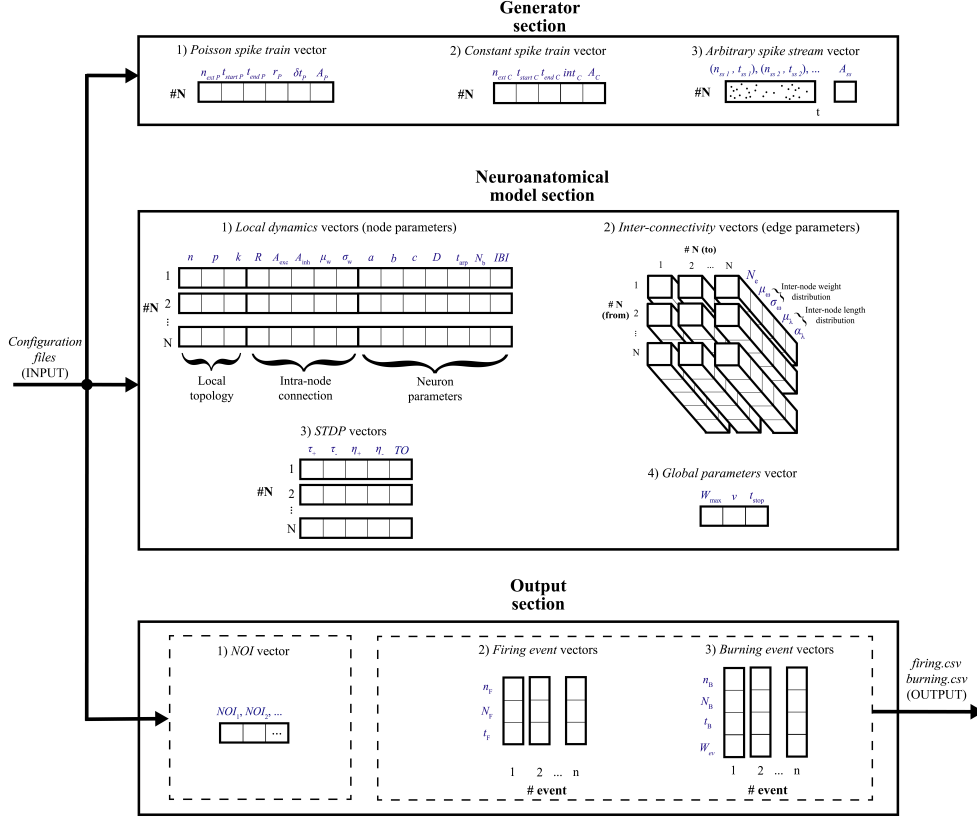


Figure 7. FNS framework overall structure. The reader can find the means of the abbreviations in Table 1

below the value W_{max} .

The *STDP vector* (i.e., **STDPV**) contains all STDP parameters discussed in Sect. 2.5 and defines the STDP to act on a specific node.

The global parameters of the system are defined by the *global parameters vector* (i.e., **GPV**). Among these, t_{stop} specifies the neural activity time we want to simulate in biological time units (ms).

3.3. Output section

This section allows the user to choose regions and type of contributions for which to extract information. Before the simulation starts, the user can specify

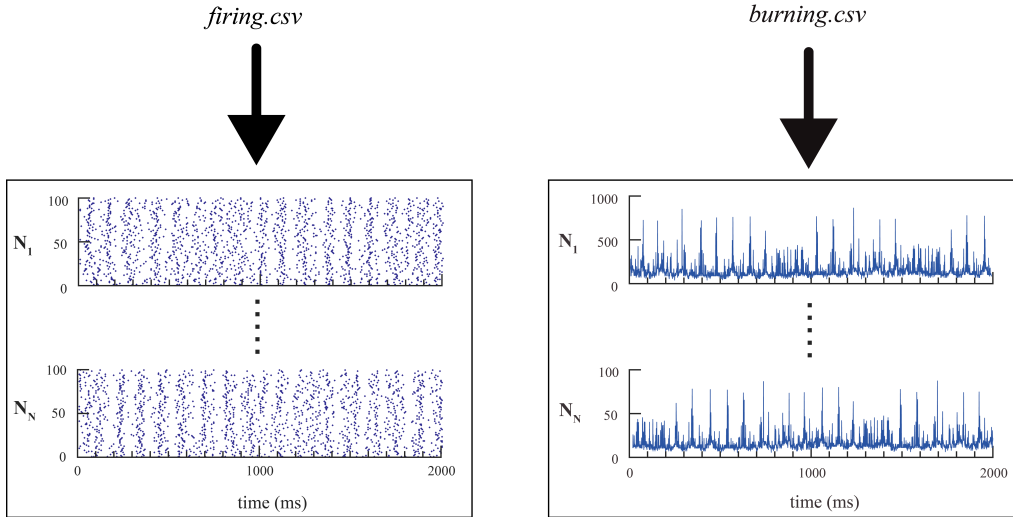


Figure 8. Two seconds of simulated electrophysiological signal extracted from *firing.CSV* and *burning.CSV* files (spike rasterplot and postsynaptic activity, respectively) of a simulation of N_N nodes, composed of 100 neurons each. The figures have been obtained through the Matlab® script available on the FNS website.

the list of nodes for which to store all simulation data (*nodes of interests*, or NOIs) through the *NOI vector* (i.e., \mathbf{NV}). At the end of the simulation, data of all firing and burning events in which such NOIs are implicated are available to the user, in form of a vector for each event. Depending whether it is a firing or burning event, in the output we obtain different vectors: *firing event vector* (i.e., \mathbf{FV}) or *burning event vector* (i.e., \mathbf{BV}), respectively. Such vectors are collected and made available to the user through the two files *firing.CSV* and *burning.CSV*. The former reports exhaustive information on firing events and burning events, respectively, to extract simulated electrophysiological signal (firing activity in the first case and postsynaptic activity in the second case), see Fig. 8.

4. Implementation aspects

When a simulation is launched in FNS, two phases are performed in sequence: the first phase consists in the *initialization* of the data structures

needed by the simulation; the second phase consists in the actual *simulation* of events.

The first phase is carried out through the following steps:

- reading of the *Generator section* and *Neuroanatomical model section* configuration vectors, and the list of NOIs for which the event vectors *FV* and *BV* (of *Output section*) have to be stored;
- creation of the node-specific data structures and neuron clusters to be run concurrently;
- creation of the global data structures.

After those steps have been accomplished, the second phase begins. The parallelization strategy implemented allows the program to proceed through the sequential simulation of single slices of simulated time with a specific and constant duration, for multiple nodes at the same time. Each cycle terminates with the synchronization between nodes whose events affects each other.

4.1. Data structures

During the initialization phase the program generates the sets of values of weights and delays of the network. Possible values arising from the distributions that are negative or $> W_{max}$ are notified and rectified (see Sect. 3.2). Below we briefly describe the main data structures used by the software, highlighting which of these act at the node level:

inter-connection dictionary: it is a map containing weight and length of each inter-node connection. The connection is identified by the pre-synaptic neuron (pertaining to node A) and the post-synaptic neuron (pertaining to node B , with $B \neq A$);

intra-connection dictionary (node-specific): this is the intra-node equivalent of the *inter-connection* dictionary, where each entry represents the

weight of an intra-node connection. The connection is identified by the pre-synaptic neuron and the post-synaptic neuron (pertaining to the same node);

state dictionary (node-specific): it contains the inner states of the neurons pertaining to a specific node, and it is constantly updated through the node simulation;

active neuron list (node-specific): list of neurons in active mode pertaining to a specific node, sorted on their firing time; this list is constantly updated through the node simulation;

outgoing spike list (node-specific): lists of output pulses, including post-synaptic neuron, node and instant, generated from a specific node within a specific time slice;

STDP timing list: it temporarily stores event timings in order to compute the ΔW . Such timings are automatically discarded after the TO value defined by the user.

4.2. Event-driven procedure

An asynchronous or event-driven algorithm allows the simulation to "jump" from an event to the next one. If the SNN was characterized by identical transmission delays and absence of spike latency, the data structure would be just a *First In First Out* queue, which has fast implementations (Cormen et al., 2001). Although the neuronal and connectivity features of FNS require more complex data structures (as shown in Sect. 4.1), the simulation procedure is quite simple.

At any instant, each network neuron is characterized by its inner state, and active neurons are also characterized by their proper t_f . When a firing event occurs, it propagates toward the target neurons taking into account the connection delays (if present). Such events modify the inner state of post-synaptic neurons (and their t_f , for the active neurons), on the basis of

the amplitude and sign of the pulse, and the time elapsed from the last state update. Four different cases of state update can happen to the target neuron:

- *passive-to-passive*. This does not have any effect on the event list
- *passive-to-active*. This elicits the insertion of an event (and related firing time) orderly on the event list
- *active-to-active* (i.e., post-trigger anticipation/postponement). This elicits the update (and reordering) of its firing time on the event list
- *active-to-passive* (i.e., post-trigger inhibition). This elicits the elimination of an event (and related firing time) from the event list

In addition to the four cases listed, two “forbidden” cases can occur during the simulation: from *passive mode* to $S < 0$ and from *active mode* to $S \geq S_{max}$; for such cases, specific actions are included in the procedure (state value correction and output spike production, respectively).

At the same time, weights for which plasticity is active are updated accordingly, taking in account the *STDP timing list*.

4.3. Parallelization

In a parallel computing scenario the problem is splitted in many sub-problems such that their solutions can be computed independently and then collected to provide the global solution. In simulations of brain networks it is not trivial to determine which events can be executed in parallel because of the intricate cause-effect relations between the network elements. This led to the development of specific strategies for parallelising event-driven SNNs avoiding causality errors (e.g. D’Haene, 2006; Mouraud and Puzenat, 2009; Lobb et al., 2005; Grassmann and Anlauf, 1998; Djurfeldt et al., 2005; Delorme and Thorpe, 2003).

The event-driven parallelization method on which FNS is based on can be defined as *adaptive* (D’Haene, 2006), since the algorithm chooses an

appropriate network-specific interval of simulated time to be used for the synchronization of the parallel tasks, avoiding as much as possible the underuse of available hardware resources. Given a generic network, the *opaque period* (OP) is the minimum simulated time needed by a signal to travel from a network element to an adjacent one (Lubachevsky, 1989). Then, within any simulated time window smaller than the OP of the network, each event cannot be caused by (or cannot affect to) any other event happened during the same time window.

If ev_i and ev_j are two distinct events such as

$$|\tau(ev_j) - \tau(ev_i)| < OP, \quad i \neq j \quad (11)$$

then they can be computed in parallel without loss of cause-effect relationship. This allows us to parallelize the computation within the *time slice* $T_s < OP$. On the other hand, each unit must wait until each of the others has ended to simulate the events of the previous T_s to process new information; then, a *sync step* is needed to "deliver" the events just calculated to the unit which should use them to produce new events during the next *OPs*.

In the case of neural computation, an event could affect another one in a very short time, leading to a short *OP*, then counteracting the benefit of the parallelization. In order to efficiently perform parallel computation, in FNS the following strategy is adopted:

- each node is assigned to a specific *thread* (i.e., a process that deals with a local problem);
- the T_s duration is sized as the minimum among all the network inter-node connection delays (that we define *Bounded Opaque Period* (BOP)), since this is the shortest interval needed by a neuron of a node to affect the state of a neuron of another node.
- inter-node spikes in queue are delivered to the corresponding threads

through the *synch step*, at intervals equals to the BOP. Once a thread gets a spike event from a node, it puts this event orderly to the internal node-specific *active neuron list* and updates the internal state of the post-synaptic neuron at the proper time.

If the network presents two or more inter-connected nodes with zero-delay, FNS considers such nodes as a single *group*, and the mechanism continues to be valid. The fact of considering the more ample concept of group instead that of node enables the possibility of representing heterogeneous regions without losing the parallelization feature (see Sect. 2.3).

Threads are executed in parallel by the *thread workers* (i.e., multi-threaded or hyperthreaded CPUs), each of which can execute at most a thread at a time. In order to minimize the processing times, each worker can serve queued threads in turns for a short time, and different workers can swap threads each other, to achieve a dynamic balancing of the computational load.

Once **ICV**s (and then, the groups) have been defined, we can simulate the neural activity within each group. Each *thread* can assume one of the three states *running*, *waiting* or *runnable*. When the whole simulation starts, the steps until the completion of the execution are the following:

1. all threads are set as *runnable*;
2. each of them simulates the generation of events within the (simulated) BOP_1 (i.e., the time window from time $t = 0$ to time $t = \bar{B}$). If empty threads occur, for them the simulation jumps directly to point 3;
3. once a thread has generated all the events within the current BOP_1 window, it sets its status to *waiting*;
4. once all threads have completed to simulate the events of the BOP_1

window, all threads synchronize each other through the synch step;

5. all threads get again to the state *runnable* and simulate the events generated within the BOP_2 (i.e., the time window from time $t = \bar{B}$ to time $t = 2\bar{B}$), and so on.

This algorithm cycles until the stop condition set on the overall simulated time t_{stop} .

Obviously, a firing event generated within BOP_n not necessarily will be delivered as burning event during BOP_{n+1} : it could be delivered in one of the following BOPs, depending on the connection delay involved.

The concept of parallelization through BOP is summarized in Fig. 9, where for simplicity we consider the simple *resonance pair* motif (Gollo et al., 2014; Maslennikov and Nekorkin, 2014) (i.e., two nodes bidirectionally connected with delay).

In *Appendix D* we report a description in pseudo-code of the procedure implemented in FNS, supporting the synchronization mechanism between nodes.

5. Reproduction of spontaneous MEG functional connectivity

In order to reproduce subject specific brain’s spontaneous electrophysiological activity using FNS, both structural and functional *connectomes* (i.e., the maps of structural and functional connections within brain areas (Fornito et al., 2016)) have been extracted from a healthy participant using DTI and source-space MEG, respectively. Connectomes have been estimated using 14 regions (7 regions per hemisphere, see table 2) composing the Default Mode Network (Raichle et al., 2001; de Pasquale et al., 2010), a *task-negative* resting state network, which is more strongly active during idling states than during task performance. The participant’s structural connectivity was used

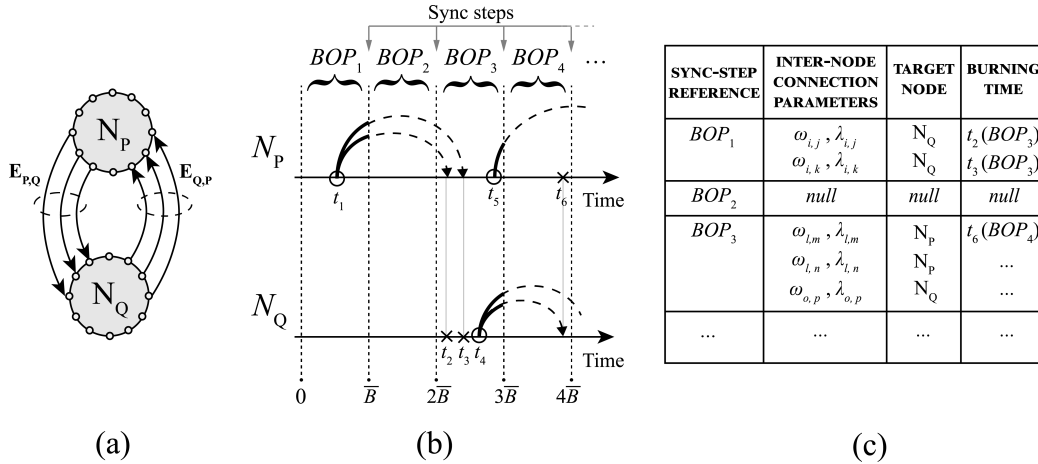


Figure 9. BOP-based parallelization mechanism. (a) Example network: two interconnected nodes are generating spiking activity (under proper external stimulation, not shown in the figure). (b) Temporal diagram of the parallelization process. Inter-node pulses are represented by dashed arrows, firing events by circles, burning events by crosses. An inter-node firing event generates burning events in the target node. The delivery of the events to the burning node will happen at the end of the firing event’s BOP. Given a firing event, related burnings will happen in one (or more) following BOPs. Given a burning event, the related firing event belongs to a BOP that precedes the current one (not necessarily the previous one). The axis represents simulated time. (c) Event schedule grid.

to estimate a structural model in the simulator, and its functional connectivity was employed to fine-tune phase and model evaluation.

5.1. Simulation setup

For the simulation we used brain data of a 66 years old male, chosen by lot from the set of control participants of a previous study (Garces et al., 2014).

#	Name
1	Left precuneus
2	Right precuneus
3	Left isthmuscingulate
4	Right isthmuscingulate
5	Left inferiorparietal
6	Right inferiorparietal
7	Left superiorfrontal

8	Right superiorfrontal
9	Left middletemporal
10	Right middletemporal
11	Left anteriorcingulate
12	Right anteriorcingulate
13	Left hippocampus
14	Right hippocampus

Table 2. Description of the 7 NOI per hemisphere considered for the connectomes, obtained from the *Freesurfer* (Fischl, 2012) cortical parcellation in 66 regions (Desikan et al., 2006) such as in (Hagmann et al., 2008).

To model spontaneous activity, we adjusted the LIFL model to emulate the behaviour of real pyramidal neurons, with a maximum latency of $25ms$, chosen on the basis of the data reported in the electrophysiology database *Neuroelectro* (Tripathy et al., 2014). Neuron’s parameters have been set to the following values: $a = 1$, $b = 0$, $c = 0.04$, $t_{arp} = 2$, $D = 0.07$. An external excitatory background input is predisposed consisting of spike trains representing the noisy fluctuations observed in vivo, with amplitude chosen in such a way that an isolated neuron displays predominant spiking activity in the alpha band (i.e., 7.5-12 Hz, the frequency range that characterizes real resting state data (Abuhassan et al., 2014)). Each node is modeled with $n = 100$ neurons for a total of 1400 neurons. $R = 0.8$ as revealed by experimental observations (Izhikevich et al., 2004) and $p = 0.5$ in order to obtain small-world properties. Remaining intra-node connectivity parameters are chosen in such a way that the post-synaptic activity of the nodes preserves its peak in the alpha band, ensuring in the meantime that there is no strict periodicity of individual oscillations, and under the condition $n \gg k \gg \ln(n) \gg 1$ (as discussed in 2.3.1), obtaining $k = 30$ and $\mu_{w_{e,i}} = 0.04$. Each edge is initialized with a number of connections $N_e/N_{e,max}$ between the considered brain regions, where N_e is equal to the number of streamlines connecting two NOIs reconstructed through DTI (see Garces et al., 2014, for the method) and the denominator operates the normalization of the values in the range $[0, 1]$.

Distances between regions μ_λ have been obtained considering the Hagmann DSI data set (Hagmann et al., 2008), available as a package of *The Virtual Brain* (Sanz Leon et al., 2013).

Final structural model counts 45000 connections, for which plasticity is not active since we are reproducing a static scenario. Simulations have been repeated with two free parameters with the goal to match the resulting FC profile with the real MEG data: conduction velocity v , which has been varied in the neighborhood of the best-matching value reported in literature (i.e., 5.1 m/s, see Cabral et al., 2014; Nakagawa et al., 2014), and interconnection weights μ_ω , which we varied in a range that ensures interaction between the nodes but without altering significantly the power spectrum previously set (i.e., [0.045, 0.09]). To extract a source-space MEG comparable signal from the model, the *burning event vector* is subsequently imported in Matlab where the events are collected in contiguous bins of 1 ms of simulated time, and the simulated time-series are calculated by summing up all synaptic pulses, as in Nakagawa et al. (2014).

From the simulated activity, for each combination of v and ω we discarded initial transients and extracted 5 segments of 6 s of activity. Then we processed the trials of simulated activity in the same way of real MEG source space signal, with the method described in (Garces et al., 2014).

Finally, for both simulated and real signal we calculated the *amplitude envelope correlation* FC index (Brookes et al., 2011) between all pairs of nodes considered.

The comparison between MEG and model FC matrices is calculated through the Pearson's correlation coefficient r between the strictly upper triangular parts of alpha band FC values across all links connecting the 14 regions of interest (as in Cabral et al. (2014) and Nakagawa et al. (2014)), after the application of the Fisher-Z transform to the FC measures, due to the non-additivity of correlation coefficients (Zimmerman et al., 2003).

The model shows the best agreement with experimental data for the

optimal values $\omega = 0.080, v = 5.2$, reaching an average correlation of $r = 0.51$ between the empirical and simulated FC profiles in the alpha band (Fig. 10) considering the overall set of trials composing the time series, a result that is more than satisfactory if compared to similar studies. Interestingly, although the groups have been tuned such that isolated neurons display predominant spiking activity in the alpha band, the final model (where the groups are interconnected through weights and delays) shows notable correlation values between MEG and model FC values also in other bands. In fact, using the optimal values $\omega = 0.085$ and $v = 5.2$, we have that $r > 0.35$ both in theta and beta bands, indicating the presence of multi-rhythmic activity, in agreement with real data (the complete set of simulation results is published on the Github page of FNS).

For the synthesis of MEG-like signals from the model, two major simplifications have been made:

- regarding the spatial organization of cortical neurons, we consider that pyramidal cells contribute the most to signal generation, taking into account that it is sufficient to reproduce the post-synaptic currents correctly, as shown in previous work (see Mazzoni et al., 2008, for an in-depth discussion on these aspects);

- the resulting signal more directly corresponds to a simulated LFP than to MEG. Nevertheless, a good correspondence between them has been reported (Nakagawa et al., 2014; Zhu et al., 2009) due to the fact that both signals arise from the same process (i.e., post-synaptic currents) (Buzsaki et al., 2012; Susi et al., 2018b).

Although the comparison shows that the model is successful in reproducing the FC strength measured in real resting state MEG data, FNS offers many possibilities for improving the model in order to achieve a better comparison, i.e., to consider a larger brain network, to use of a higher parcellation resolution, or to enhance diversity among the modules on the basis of real data.

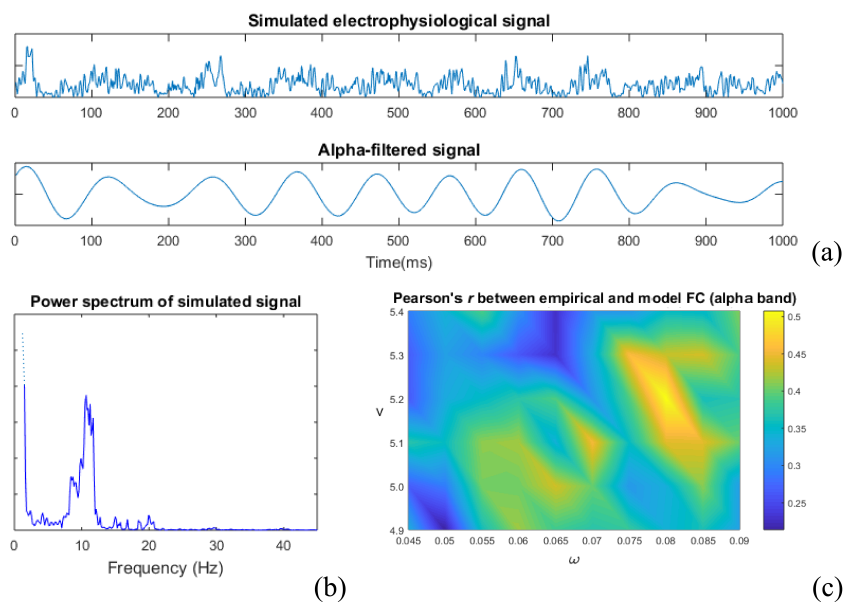


Figure 10. One second of simulated electrophysiological post-synaptic signal extracted from one node of the model with related alpha-filtered counterpart (a); power spectrum obtained from one of the trials (b); (c) represents the Pearson correlation coefficient between the simulated and the empirical FC as a function of simulation parameters v and ω . The figures have been obtained through the Matlab® script available on the FNS website.

5.1.1. Performance

Considering the example described above, the average time needed for generating a segment of 6s of simulated activity is about 100s of real time on an *Intel(R) Core(TM) i7-7700CPU @ 3.60GHz* (ram 16GB). The time needed for the initialization phase is about 2s; the remaining time is for the simulation phase. While the duration of the first phase depends on the network size only (number of neurons and connections of the network), the duration of the second phase also depends on the value of minimum inter-node length of the network. This time can be reduced by increasing the *maximum heap size* in Java (set to 8GB in these simulations). As explained in Sect. 3.3, during the simulation FNS transcribes **FV** and **BV** of the selected NOI on the two files *firing.CSV* and *burning.CSV*; the time required to do these operations depends on the number of the selected NOI (14 in this case).

6. Discussion

Dynamic models of brain networks can help us to understand the fundamental mechanisms that underpin neural processes, and to relate these processes to neural data. Among the different existing approaches, SNN-based brain simulators allow the user to perform a structure-function mapping at the level of single neurons/synapses, offering a multi-level perspective of brain dynamics. Here we have presented *FNS*, the first neural simulation framework based on the LIFL model, which combines spiking/synaptic neural modelling with the event-driven simulation technique, able to support real neuroanatomical schemes. FNS allows us to generate models with heterogeneous regions and fibre tracts (initializable on the basis of real structural data), and synaptic plasticity; in addition, it enables the introduction of various types of stimuli and the extraction of outputs at different network stages, depending on the kind of activity to be reproduced. With the aim of showing to the reader a simulation example, we have synthesized a subject-specific brain model sized on real structural data, and analyzed the network

spontaneous activity; the comparison with real MEG data shows that FNS is able to reproduce satisfactorily the patterns of neuromagnetic brain sources. In addition, although the nodes have been tuned to oscillate prominently in the alpha band, in the final model there are quite relevant correlation values between MEG and model FC also in other bands (as theta and beta bands), testifying the presence of multirhythmic activity, in agreement with experimental data. This indicates that the spike latency feature could be a key-aspect to reproduce cross-frequency interactions.

FNS is downloadable for free and allows the researcher to face realistic simulations, with limited time and budget. The current version of the software is written in Java[®] and the parallelization is currently implemented as a *multi-threaded* Java standalone application, taking advantage that Java presents specific features oriented to the optimization of memory resources (i.e., the *Java Garbage Collector*), and native support for parallel computation (Ponge, 2011). Future improvements include:

- translation of our framework to hybrid CPU-GPU technologies (e.g., *CUDA*) or cloud computing scenarios (e.g., *MapReduce*);
- development of an user-friendly interface and improvement of the compatibility with existent FC estimation tools (e.g., *Hermes* (Niso et al., 2013));
- development of a version of FNS based on low level programming languages (e.g., *C* or *GO*) to improve performances and compatibility with *high performing computing* platforms;
- considering the use of look-up tables (Reutimann et al., 2003; Naveros et al., 2017) to characterize neuronal dynamics of the LIFL model, for further speeding up simulations. In this process attention must be paid to the insertion of timing errors (Ros et al., 2006) to not to compromise some *temporal coding*-based LIFL applications, as Susi et al. (2018a).

Although a simulation test has been conducted and commented, this document is not intended as user guide, but as an explanation of the mathematical operation and structure of the simulator. The reader can find the software package and technical documentation on the FNS website: www.fnsneuralsimulator.org

7. Supplementary material

Appendix A: LIFL Features

LIFL neuron supports natively the following neurophysiological properties: *integrator*, *spike latency*, *tonic spiking* and *class 1 excitability*, obtained by the implementation of the neuron equations in MATLAB environment. Among these:

- *Tonic Spiking* takes place when a neuron fires a continuous spike train when stimulated through a DC current input (Izhikevich, 2004). We show this property stimulating a single neuron with a constant spike train (i.e., a discretized DC current input) with amplitude A_c . The raster plot of the spiking neuron activity (i.e., the output neuron response) is reported in Fig. B1. Note that the firing frequency of the neuron is constant.
- *Class 1 Excitability*, exhibited by some cortical neurons, allows the neuron to spike with a frequency that depends on the input strength (ranging from 2 Hz to 200 Hz or more), including the fire at low-frequency when the input is weak. This property allows neurons to encode the input strength into their firing rate (Izhikevich, 2004). In Fig. B1, we show this behavior stimulating a neuron with a ramp input. Of course, in this case the firing frequency of the neuron is not constant.

In order to further improve the realism of the LIFL neuron, some adjustments can be made at the programming level (as done for the *refractory*

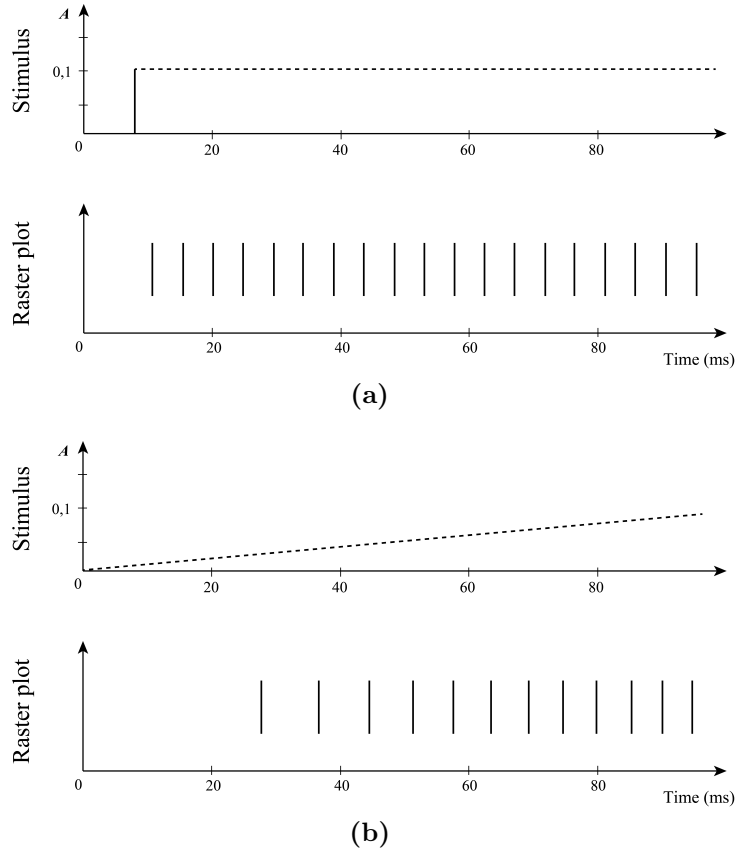


Figure B1. (a): *Tonic Spiking* behavior of LIFL neuron (basic configuration). Top: *DC* input stimulus with $A_c = 0.1$. Bottom: raster plot (firing activity) of the stimulated neuron, with respect to (simulated) biological time.

(b): *Class 1 Excitability* behavior of LIFL neuron (basic configuration). Top: *ramp* input stimulus with slope = 0.001. Bottom: raster plot (firing activity) of the stimulated neuron, with respect to (simulated) biological time.

Note that, in order to introduce the external inputs to the event-driven system, we used discrete versions of DC and ramp signals, sampled at constant intervals of $dt = 0.1$ model time

period and the *tonic bursting*), obtaining other computational features as, for example *mixed mode*(Izhikevich, 2004).

With regards to the underthreshold decay, FNS gives the possibility to choose among:

- Linear decay:

Assuming $T_l = D\Delta t$, in which D is the *decay parameter*, and Δt represents the temporal distance between a couple of consecutive incoming spikes (of course, $D \geq 0$; for $D = 0$ no decay is applied in passive mode, and the neuron behaves as a *perfect integrator*).

- Exponential decay:

Assuming $T_l = S_{p_j} \cdot (1 - e^{-\Delta t/D})$, obtaining for the overall update equation:

$$S_j = A_i \cdot W_{i,j} + S_{p_j} \cdot e^{-\frac{\Delta t}{D}} \quad (\text{B1})$$

in which D here represents the classic *time constant*.

Appendix B: T_r calculation

Referring to Fig. A1, at the time the neurons inner state is altered from a second input (here excitatory, but non influential to calculation purposes), the *intermediate state* S_i is determined, and then T_r is calculated.

In event-driven, network elements are updated only when they receive or emit a spike. Once an input spike arrives in active mode, the S_i is calculated on the basis of the time remaining to the spike generation.

Referring to the generic inner state S_i the firing equation is:

$$t_{f,i} = \frac{a}{S_i - 1} - b \quad (\text{A1})$$

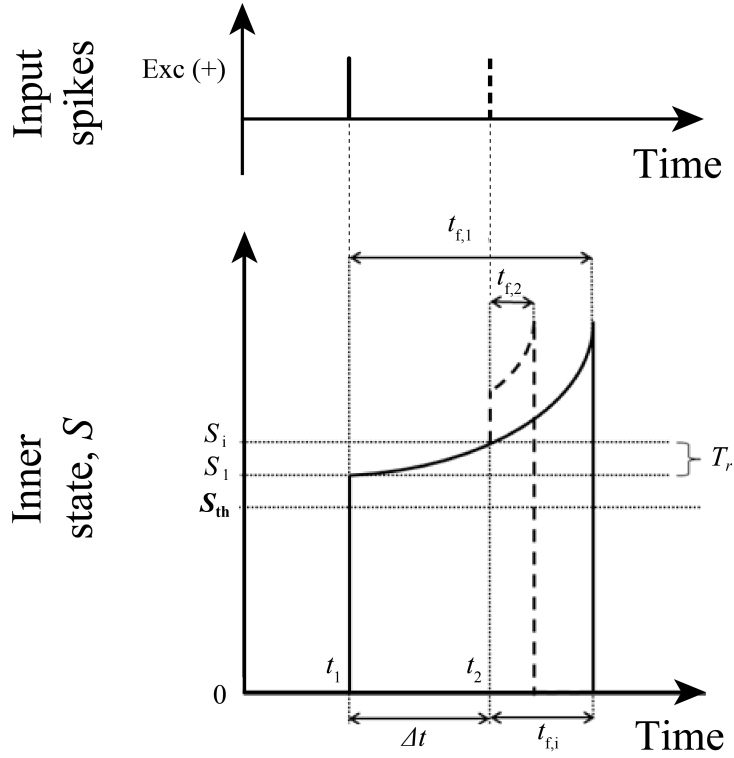


Figure A1. Representation of T_r . LIFL neuron in active mode is characterized by a spontaneous growth of S . If a pulse arrives before the actual spike generation, S is modified and the t_f will be recalculated. The recalculation considers the intermediate state S_i , i.e., the neuron state at the time the pulse arrives.

We define:

$$\Delta t = t_2 - t_1 \quad (\text{A2})$$

where t_1 and t_2 represent the arrival instants of the synaptic pulses to the considered neuron. Then:

$$t_{f,i} = t_{f,1} - \Delta t \quad (\text{A3})$$

Rearranging Eq. A1, we obtain:

$$S_i = \frac{a}{t_{f,i} + b} + 1 \quad (\text{A4})$$

Now we combine Eq. A3 with Eq. A4

$$S_i = \frac{a}{t_{f,1} - \Delta t + b} + 1 \quad (\text{A5})$$

By defining

$$T_r = S_i - S_1 \quad (\text{A6})$$

where

$$S_1 = \frac{a}{(t_{f,1} + b)} + 1 \quad (\text{A7})$$

and putting Eq. A5 and A7 in A6, we obtain:

$$T_r = \frac{a}{t_{f,1} - \Delta t + b} - \frac{a}{t_{f,1} + b} \quad (\text{A8})$$

that can be rearranged as

$$T_r = \frac{a\Delta t}{(t_{f,1} + b - \Delta t)(t_{f,1} + b)} \quad (\text{A9})$$

Note that we are interested in determining an intermediate state; this implies that we consider the second synaptic pulse only if its timing (i.e., t_2) falls before the spike occurs. This gives us:

$$\Delta t < t_{f,1} \quad (\text{A10})$$

thus we do not have restrictions from the denominator of A9.

The relation A9 can be generalized to the case as more input modify the firing time; then, we can write

$$T_r = S_{ic} - S_{ip} = \frac{a\Delta t_i}{(t_{f,ip} + b - \Delta t_i)(t_{f,ip} + b)} \quad (\text{A11})$$

with

$$\Delta t_i = t_{ic} - t_{ip} \quad (\text{A12})$$

where the subscript *ip* stays for *intermediate-previous* and *ic* for *intermediate-current*.

We can also make explicit the dependence of T_r from the previous state, by inverting $t_{f,ip}$ through Eq. A1, obtaining:

$$T_r = \frac{(S_{ip} - 1)^2 \Delta t}{a - (S_{ip} - 1) \Delta t} \quad (\text{A13})$$

Obviously, the same considerations on the arrival time of the second pulse remain valid, thus we do not have restrictions imposed by the denominator of A13.

Appendix C: types of distributions used in the model

In FNS Gaussian distributions are implemented both for the initialization of intra-module weights of modules (one set for excitatory and one set for inhibitory) and inter-module weights of each edge:

$$f(W) = \frac{1}{\sqrt{2\pi\sigma_W^2}} \exp\left(\frac{(W - \mu_W)^2}{-2\sigma_W^2}\right) \quad (\text{C1})$$

where μ_W is the mean, and σ_W^2 is the variance of the distribution. In the formula, W is intended to represent A (distribution of intra-module weights) or ω (distribution of intermodule weights).

In time, a gamma distribution is implemented for inter-module lengths, which reflects on a gamma distribution of delays. Such gamma distribution is characterized from parameters μ_λ (i.e., *mean parameter*) and α_λ (i.e., *shape parameter*). If we call λ the (axonal) delay, the probability density function of a gamma distribution can be written as:

$$f(\lambda) = \lambda^{\alpha_\lambda - 1} \frac{\exp(-\lambda\alpha_\lambda/\mu_\lambda)}{(\mu_\lambda/\alpha_\lambda)^{\alpha_\lambda} \Gamma(\alpha_\lambda)} \quad (\text{C2})$$

Note that μ_λ can be defined as:

$$\mu_\lambda = \alpha_\lambda \theta \tag{C3}$$

where θ is known as the *scale parameter*.

Note that with the parameter α_λ is possible to control the type of distribution (low α_λ values lead toward the exponential distribution; high α_λ values lead toward the Dirac distribution); the more α_λ is high, the more the distribution *mode* approaches μ_λ (from the left).

Appendix D: Pseudo-code procedure

- let `spike_queue` be the list of all spikes generated by any pre-synaptic neuron sorted in ascending order of spike time (the first spike in the list is the one with the least spike time);
- let `outer_burning_event`: the list of spikes to be delivered to post-synaptic neurons belonging to outer nodes. At each synchronization:
 1. each entry of this list is read and sent to the thread executing the routine for the right node;
 2. after each item in the list has been sent, the whole list is cleared.
- let `current_time` be the current simulated time;
- let `split_stop_time` be the stop time for the current BOP simulation;
- let `final_stop_time` be the simulated time at which the whole simulation must stop;
- let `run_burning_routine(s*)` be the routine which calculates all the burning events caused by the fire event hold by the spike `s*`: during this procedure, all the burning events involving post-synaptic neurons of outer nodes are stored to a special `outer_burning_event`;

- let `send_fires_for_outer_nodes()` be the routine which sends the spikes stored in `outer_burning_event` to post-synaptic neurons in outer nodes;
- let `update_incoming_spikes_queue()` be the routine which updates the `spike_queue` with the spikes coming from outer nodes and targeting post-synaptic neurons of the present node before beginning the next BOP simulation.

```

while true:
    while current_time < split_stop_time:
        s* = spike_queue.pop()
        run_burning_routine(s*)
        if current_time >= split_stop_time:           (1)
            if split_stop_time >= final_stop_time:   (2)
                return
            send_fires_for_outer_nodes()
            wait_until(current_time < split_stop_time) (3)
    update_spikes_queue()

```

(1) end of the BOP: send the fires to the outer nodes

(2) end of the last BOP: end of the node simulation

(3) stops the thread until `split_stop_time` is updated with the next BOP stop time

Information Sharing Statement

Software, simulation results and new network models are available at the FNS official website [www.fnsbrainsimulator.org] and GitHub page [<https://github.com/fnsneuralsimulator>].

References

References

- P. Hagmann. *From diffusion MRI to brain connectomics*. Dissertation, Lausanne: EPFL, 2005. URL <https://infoscience.epfl.ch/record/33696>.
- C. Sporns, G. Tononi, and R. Kötter. The human connectome: A structural description of the human brain. *PLoS Computational Biology*, 1(4), 09 2005. URL <https://doi.org/10.1371/journal.pcbi.0010042>.
- A. Barardi, B. Sancristbal, and J. Garcia-Ojalvo. Phase-coherence transitions and communication in the gamma range between delay-coupled neuronal populations. *PLoS Computational Biology*, 10(7):e22561, 2014. doi: 10.1371/journal.pcbi.1003723. URL <https://doi.org/10.1371/journal.pcbi.1003723>.
- J. Cabral, E. Hugues, O. Sporns, and G. Deco. Role of local network oscillations in resting-state functional connectivity. *Neuroimage*, 57(1), 2011.
- G. Deco and V.K. Jirsa. Ongoing cortical activity at rest: Criticality, multistability, and ghost attractors. *The Journal of Neuroscience*, 32(10):3366–3375, 2012.
- RG Bettinardi, G Deco, VM Karlaftis, TJ Van Hartevelt, HM Fernandes, Z Kourtzi, ML Kringelbach, and G. Zamora-Lpez. How structure sculpts function: Unveiling the contribution of anatomical connectivity to the brain’s spontaneous correlation structure. *Chaos*, 27(4), 2017.
- T.T. Nakagawa, M. Woolrich, H. Luckhoo, M. Joensson, H. Mohseni, M.L. Kringelbach, V Jirsa, and G. Deco. How delays matter in an oscillatory whole-brain spiking-neuron network model for MEG alpha-rhythms at

- rest. *Neuroimage*, 87:383–394, 2014. URL <https://doi.org/10.1016/j.neuroimage.2013.11.009>.
- J. Cabral, H. Luckhoo, M. Woolrich, M. Joensuu, H. Mohseni, A. Baker, M.L. Kringelbach, and G. Deco. Exploring mechanisms of spontaneous functional connectivity in MEG: How delayed network interactions lead to structured amplitude envelopes of band-pass filtered oscillations. *Neuroimage*, 90: 423–435, 2014. URL <https://doi.org/10.1016/j.neuroimage.2013.11.047>.
- Gustavo Deco, Joana Cabral, Mark W. Woolrich, Angus B.A. Stevner, Tim J. van Hartevelt, and Morten L. Kringelbach. Single or multiple frequency generators in on-going brain activity: A mechanistic whole-brain model of empirical meg data. *Neuroimage*, 152:538–550, 2017.
- G. Deco, V.K. Jirsa, P. A. Robinson, M. Breakspear, and K.l. Friston. The dynamic brain: From spiking neurons to neural masses and cortical fields. *PLOS Comput Biol*, 4:1–35, 2008. URL <https://doi.org/10.1371/journal.pcbi.1000092>.
- R. Vicente, L. L. Gollo, C. R. Mirasso, I. Fischer, and G. Pipa. Dynamical relaying can yield zero time lag neuronal synchrony despite long conduction delays. *Proceedings of the National Academy of Sciences USA*, 105(44): 17157–17162, 2008.
- L Gollo, C Mirasso, and A Villa. Dynamic control for synchronization of separated cortical areas through thalamic relay. *NeuroImage*, 52(3):947–955, 2010. doi: 10.1016/j.neuroimage.2009.11.058. URL <https://doi.org/10.1016/j.neuroimage.2009.11.058>.
- Oleg V. Maslennikov and Vladimir I. Nekorkin. Modular networks with delayed coupling: Synchronization and frequency control. *Phys. Rev. E*, 90:012901, Jul 2014. doi: 10.1103/PhysRevE.90.012901.

JW Bohland, C Wu, H Barbas, H Bokil, M Bota, HC Breiter, HT Cline, JC Doyle, PJ Freed, RJ Greenspan, SN Haber, M Hawrylycz, DG Herrera, CC Hilgetag, ZJ Huang, A Jones, EG Jones, HJ Karten, D Kleinfeld, R Ktter, HA Lester, JM Lin, BD Mensh, S Mikula, J Panksepp, JL Price, J Safdieh, CB Saper, ND Schiff, JD Schmahmann, BW Stillman, K Svoboda, LW Swanson, AW Toga, DC Van Essen, JD Watson, and PP Mitra. A proposal for a coordinated effort for the determination of brainwide neuroanatomical connectivity in model organisms at a mesoscopic scale. *PLoS Computational Biology*, 5(3):1–9, 2009. doi: 10.1371/journal.pcbi.1000334. URL <https://doi.org/10.1371/journal.pcbi.1000334>.

E. M. Izhikevich. Which model to use for cortical spiking neurons? *IEEE Transaction on Neural Networks*, 15(5):1063–1070, 2004.

R. Brette, M. Rudolph, T. Carnevale, H. Hines, D. Beeman, J. M. Bower, M. Diesmann, A. Morrison, P. H. Goodman, F. C. Jr Harris, M. Zirpe, T. Natschläger, D. Pecevski, B. Ermentrout, M. Djurfeldt, A. Lansner, O. Rochel, T. Vieville, E. Muller, A. P. Davison, S. El Boustani, and A. Destexhe. Simulation of networks of spiking neurons: A review of tools and strategies. *Journal of Computational Neuroscience*, 23(3):349–398, 2007.

A. Hanuschkin, S. Kunkel, M. Helias, A. Morrison, and M. Diesmann. A general and efficient method for incorporating precise spike times in globally time-driven simulations. *Frontiers in Neuroinformatics*, 4(113), 2010. doi: 10.3389/fninf.2010.00113. URL <https://doi.org/10.3389/fninf.2010.00113>.

J Krishnan, P Porta Mana, M Helias, M Diesmann, and E. Di Napoli. Perfect detection of spikes in the linear sub-threshold dynamics of point neurons. *Frontiers in Neuroinformatics*, 11(75), 2017.

Anthony Mouraud and Didier Puzenat. Simulation of large spiking neural

- networks on distributed architectures. the DAMNED simulator. In Dominic Palmer-Brown, Chrisina Draganova, Elias Pimenidis, and Haris Mouratidis, editors, *Engineering Applications of Neural Networks.*, pages 359–370. Springer International Publishing, 2009. ISBN 978-3-642-03968-3. doi: 10.1007/978-3-642-03969-0_33.
- E. Ros, R. Carrillo, E.M. Ortigosa, B. Barbour, and R. Agís. Event-driven simulation scheme for spiking neural networks using lookup tables to characterize neuronal dynamics. *Neural Computation*, 18(12):2959–2993, 2006.
- R. Brette. Exact simulation of integrate-and-fire models with synaptic conductances. *Neural Computation*, 18(8):2004–2027, 2006.
- R. Brette. Exact simulation of integrate-and-fire models with exponential currents. *Neural Computation*, 19(10):2604–2609, 2007.
- A Tonnelier, H Belmabrouk, and D Martinez. Event-driven simulations of nonlinear integrate-and-fire neurons. *Neural Comput.*, 19(12):1426–1461, 2007. doi: 10.1162/NECO_a_00278.
- M. Salerno, G. Susi, and A. Cristini. Accurate latency characterization for very large asynchronous spiking neural networks. In M. Pellegrini, A. L. N. Fred, J. Filipe, and H. Gamboa, editors, *BIOINFORMATICS 2011 - Proceedings of the International Conference on Bioinformatics Models, Methods and Algorithms*, pages 116–124. SciTePress, 2011.
- M Rudolph-Lilith, M Dubois, and A Destexhe. Analytical integrate-and-fire neuron models with conductance-based dynamics and realistic postsynaptic potential time course for event-driven simulation strategies. *Neural Comput.*, 24(6):1426–1461, 2012. doi: 10.1162/NECO_a_00278.
- D. Pecevski, D. Kappel, and Z. Jonke. NEVESIM: event-driven neural simulation framework with a python interface. *Frontiers in Neuroinformatics*,

- 8(70), 2014. ISSN 1662-5196. doi: 10.3389/fninf.2014.00070. URL <http://journal.frontiersin.org/article/10.3389/fninf.2014.00070>.
- A. Cristini, M. Salerno, and G. Susi. A continuous-time spiking neural network paradigm. In S. Bassis, A. Esposito, and F. C. Morabito, editors, *Advances in Neural Networks: Computational and Theoretical Issues*, pages 49–60. Springer International Publishing, 2015. ISBN 978-3-319-18163-9. doi: 10.1007/978-3-319-18164-6_6.
- A Morrison, S Straube, H Plesser, and M Diesmann. Exact subthreshold integration with continuous spike times in discrete time neural network simulations. *Neural Computation*, 19:47–79, 2006.
- M D’Haene, M Hermans, and B Schrauwen. Toward unified hybrid simulation techniques for spiking neural networks. *Neural Comput.*, 26(6):1055–79, 2014. doi: 10.1162/NECO_a.00587.
- M. Gewaltig and M. Diesmann. NEST (NEural Simulation Tool). *Scholarpedia*, 2(4):1430, 2007.
- R. Brette and D. Goodman. *Brian Documentation. Release 1.4.3*, 2016. URL <http://www.briansimulator.org>.
- Gianluca Susi, Luis Antn Toro, Leonides Canuet, Maria Eugenia Lpez, Fernando Maest, Claudio R. Mirasso, and Ernesto Pereda. A neuro-inspired system for online learning and recognition of parallel spike trains, based on spike latency, and heterosynaptic stdp. *Frontiers in Neuroscience*, 12:780, 2018a. ISSN 1662-453X. doi: 10.3389/fnins.2018.00780.
- G. C. Cardarilli, A. Cristini, L. Di Nunzio, M. Re, M. Salerno, and G. Susi. Spiking neural networks based on LIF with latency: Simulation and synchronization effects. In *2013 Asilomar Conference on Signals, Systems and Computers*, pages 1838–1842, Pacific Grove, CA, USA, 2013. IEEE.

- G. Susi. Bio-inspired temporal-decoding network topologies for the accurate recognition of spike patterns. *Transactions on Machine Learning and Artificial Intelligence*, 3(4):27–41, 2015. doi: 10.14738/tmlai.34.1438.
- G. Susi, A. Cristini, and M. Salerno. Path multimodality in Feedforward SNN module, using LIF with latency model. *Neural Network World*, 26(4): 363–376, 2016.
- S. Acciarito, G.C. Cardarilli, A. Cristini, L. Di Nunzio, R. Fazzolari, G.M. Khanal, M. Re, and G. Susi. Hardware design of LIF with latency neuron model with memristive STDP synapses. *Integration, the VLSI Journal*, 59: 81–89, 2017. ISSN 0167-9260.
- R. FitzHugh. Mathematical models of threshold phenomena in the nerve membrane. *Bulletin of Mathematical Biology*, 17(4):257–278, 1955.
- JP Thivierge. Neural diversity creates a rich repertoire of brain activity. *Communicative & Integrative Biology*, 1:188–189, 2008.
- LL. Gollo, M. Copelli, and J. A. Roberts. Diversity improves performances in excitable networks. *PeerJ*, 4:e1912, 2016. URL <https://doi.org/10.7717/peerj.1912>.
- N Brunel and V. Hakim. Fast global oscillations in networks of integrate-and-fire neurons with low firing rates. *Neural computation*, 11(7):1621–71, 1999.
- N Brunel and X.J. Wang. What determines the frequency of fast network oscillations with irregular neural discharges? i. synaptic dynamics and excitation-inhibition balance. *Journal of Neurophysiology*, 90(1):415–30, 2003.
- A Viriyopase, I Bojak, M Zeitler, and S Gielen. When long-range zero-lag synchronization is feasible in cortical networks. *Frontiers in computational*

- neuroscience*, 6:49, 2012. URL <https://www.frontiersin.org/article/10.3389/fncom.2012.00049>.
- LL Gollo, C Mirasso, O Sporns, and M Breakspear. Mechanisms of zero-lag synchronization in cortical motifs. *PLOS computational biology*, 10(4): 1–17, 2014. doi: 10.1371/journal.pcbi.1003548. URL <https://doi.org/10.1371/journal.pcbi.1003548>.
- K Abuhassan, D Coyle, and L Maguire. Compensating for thalamocortical synaptic loss in Alzheimer’s disease. *Frontiers in computational neuroscience*, 8(65), 2014. ISSN 1662-5188. doi: 10.3389/fncom.2014.00065. URL <https://doi.org/10.3389/fncom.2014.00065>.
- E. M. Izhikevich. Simple model of spiking neurons. *IEEE Transaction on Neural Networks*, 14(6):1569–1572, 2003.
- H. Wang, Y. Chen, and Y. Chen. First-spike latency in hodgkin’s three classes of neurons. *Journal of Theoretical Biology*, 328:19–25, 2013.
- L Trotta, A Franci, and R Sepulchre. First spike latency sensitivity of spiking neuron models. *BMC Neuroscience*, 14(1):354, 2013. ISSN 1471-2202.
- E. M. Izhikevich. *Dynamical systems in neuroscience: the geometry of excitability and bursting*. Computational neuroscience. MIT Press, Cambridge, Mass., London, 2007.
- Tim Gollisch and Markus Meister. Rapid neural coding in the retina with relative spike latencies. *Science*, 319(5866):1108–1111, 2008. ISSN 0036-8075. doi: 10.1126/science.1149639. URL <http://science.sciencemag.org/content/319/5866/1108>.
- B Fontaine and H Peremans. Bat echolocation processing using first-spike latency coding. *Neural Networks*, 22(10):1372 – 1382, 2009. ISSN 0893-6080.

- Rafael D. Vilela and Benjamin Lindner. Comparative study of different integrate-and-fire neurons: Spontaneous activity, dynamical response, and stimulus-induced correlation. *Phys. Rev. E*, 80:031909, Sep 2009. doi: 10.1103/PhysRevE.80.031909. URL <http://link.aps.org/doi/10.1103/PhysRevE.80.031909>.
- N Fourcaud-Trocme, D Hansel, C van Vreeswijk, and N Brunel. How spike generation mechanisms determine the neuronal response to fluctuating inputs. *The Journal of Neuroscience*, 23(5):11628–11640, 2003. ISSN 1529-2401.
- M. Mattia and P. Del Giudice. Efficient event-driven simulation of large networks of spiking neurons and dynamical synapses. *Neural Computation*, 12(10):2305–2329, 2000.
- V.J. Barranca, D.C. Johnson, J.L. Moyher, J.P. Sauppe, M.S. Shkarayev, G. Kovacic, and D. Cai. Dynamics of the exponential integrate-and-fire model with slow currents and adaptation. *Journal of Computational Neuroscience*, 37(1):161–180, 2014.
- A. L. Hodgkin and A. F. Huxley. A quantitative description of membrane current and application to conduction and excitation in nerve. *The Journal of Physiology*, 117(4):500–544, 1952.
- M. L. Hines and N. T. Carnevale. The NEURON simulation environment. *Neural Computation*, 9(6):1179–1209, 1997.
- J. D. Watts and S. H. Strogatz. Collective dynamics of 'small-world' networks. *Nature*, 393(1):440–442, 1998.
- H Riecke, A Roxin, S Madruga, and SA Solla. Multiple attractors, long chaotic transients, and failure in small-world networks of excitable neurons. *Chaos*, 17(2), 2007. URL <https://doi.org/10.1063/1.2743611>.

- EM Izhikevich, JA Gally, and GM Edelman. Spike-timing dynamics of neuronal groups. *Cereb Cortex.*, 14(8):933–944, 2004.
- R Ton, G Deco, and A Daffertshofer. Structure-function discrepancy: Inhomogeneity and delays in synchronized neural networks. *PLOS Computational Biology*, 10(7):1–15, 2014. doi: 10.1371/journal.pcbi.1003736.
- KJ Smith. Conduction properties of central demyelinated and remyelinated axons, and their relation to symptom production in demyelinating disorders. *Nature (eye)*, 8(2):224–237, 1994.
- J. Sjöström and W. Gerstner. Spike-timing dependent plasticity. http://www.scholarpedia.org/article/Spike-timing_dependent_plasticity, 2010.
- G.Q. Bi and M.M. Poo. Synaptic modifications in cultured hippocampal neurons: dependence on spike timing, synaptic strength, and postsynaptic cell type. *The Journal of Neuroscience*, 18(24):10464–10472, 1998.
- L. F. Abbott and S. B. Nelson. Synaptic plasticity: taming the beast. *Nature Neuroscience*, 3:1178–1183, 2000.
- M. C. van Rossum, M. Shippi, and A. B. Barrett. Soft-bound synaptic plasticity increases storage capacity. *PLOS Computational Biology*, 8(12):1–11, 2012. URL <https://doi.org/10.1371/journal.pcbi.1002836>.
- N Caporale and Y Dan. Spike timing-dependent plasticity: a Hebbian learning rule. *Annu Rev Neurosci.*, 31:25–46, 2008.
- F Frohlich, M Bazhenov, and T J Sejnowski. Pathological effect of homeostatic synaptic scaling on network dynamics in diseases of the cortex. *The Journal of Neuroscience The Official Journal of the Society for Neuroscience*, 28(7):1709–1720, 2008. doi: 10.1523/JNEUROSCI.4263-07.2008.

- W. Gerstner, W.M. Kistler, R. Naud, and L. Paninski. *Neuronal Dynamics. From single neurons to networks and models of cognition*. Cambridge University Press, 2014.
- David Heeger and Professor David Heeger. Poisson model of spike generation, 2000. URL <http://citeseerx.ist.psu.edu/viewdoc/summary?doi=10.1.1.37.6580>.
- A. Mazzoni, S. Panzeri, N.K. Logothetis, and N. Brunel. Encoding of naturalistic stimuli by local field potential spectra in networks of excitatory and inhibitory neurons. *PLOS Computational Biology*, 4(12):1–20, 12 2008. URL <https://doi.org/10.1371/journal.pcbi.1000239>.
- T. Cormen, C. Leiserson, R. Rivest, and C. Stein. *Introduction to algorithms, 2nd ed.* The MIT Press, 2001.
- Michiel D’Haene. A framework for parallel event driven simulation of large spiking neural networks. In *7e FirW Doctoraatssymposium*, 2006.
- CJ Lobb, Z Chao, Fujimoto, RM, and SM Potter. Parallel event-driven neural network simulations using the hodgkin-huxley neuron model. In *Principles of Advanced and Distributed Simulation (PADS)*, pages 16–25, 2005. doi: 10.1109/PADS.2005.18.
- C Grassmann and JK Anlauf. Distributed, event driven simulation of spiking neural networks. In *Proceedings of the International ICSC - IFAC Symposium on Neural Computation*, pages 100–105, 1998.
- M Djurfeldt, C Johansson, O Ekeberg, M Rehn, M Lundqvist, and A Lansner. Massively parallel simulation of brain-scale neural network models. Technical report, “KTH” School of Computer Science and Communication, Stockholm, Sweden, 2005.

- A Delorme and SJ Thorpe. SpikeNET: an event-driven simulation package for modelling large networks of spiking neurons. *Network Computation in Neural Systems*, 14(4):613–627, 2003.
- B.D. Lubachevsky. Efficient distributed event-driven simulations of multiple-loop networks. *Communications of the ACM*, 32(1):111–123, 1989.
- A. Fornito, A. Zaleski, and E.T. Bullmore. *Fundamentals of brain network analysis*. Elsevier, 2016.
- Marcus Raichle, Ann Mary MacLeod, Abraham Z. Snyder, William J. Powers, Debra A. Gusnard, and Gordon L. Shulman. A default mode of brain function. *Proceedings of the National Academy of Sciences USA*, 98(2):676–682, 2001.
- Francesco de Pasquale, Stefania Della Penna, Abraham Z. Snyder, Christofer Lewis, Dante Mantini, Laura Marzetti, Paolo Belardelli, Luca Ciancetta, Vittorio Pizzella, Gian Luca Romani, and Maurizio Corbetta. Temporal dynamics of spontaneous MEG activity in brain networks. *Proceedings of the National Academy of Sciences USA*, 107(13):6040–6045, 2010.
- Pilar Garces, Jose-Angel Pineda, Leonides Canuet, Sara Aurtenetxe, Maria Eugenia Lopez, Alberto Marcos, Miguel Yus, Marcos Llanero-Luque, Francisco del Pozo, Miguel Sancho, and Fernando Maestú. The Default Mode Network is functionally and structurally disrupted in amnesic mild cognitive impairment - a bimodal MEG DTI study. *Neuroimage Clin.*, 6:214–221, 2014. URL <https://doi.org/10.1016/j.nicl.2014.09.004>.
- B Fischl. Freesurfer. *Neuroimage*, 62(2):774–781, 2012. doi: 10.1016/j.neuroimage.2012.01.021. URL <https://doi.org/10.1016/j.neuroimage.2012.01.021>.
- R.S. Desikan, F Segonne, B Fischl, B.T. Quinn, B.C. Dickerson, D. Blacker, R.L. Buckner, A.M. Dale, R.P. Maguire, B.T. Hyman, M.S. Albert, and R.J.

- Killiany. An automated labeling system for subdividing the human cerebral cortex on MRI scans into gyral based region of interests. *Neuroimage*, 31: 968–980, 2006. URL <https://doi.org/10.1016/j.neuroimage.2006.01.021>.
- P Hagmann, L Cammoun, X Gigandet, R Meuli, C Honey, VJ Wedeen, and O Sporns. Mapping the structural core of human cerebral cortex. *Plos Biology*, 6(7):1–15, 2008. URL <https://doi.org/10.1371/journal.pbio.0060159>.
- Shreejoy J. Tripathy, Judith Savitskaya, Shawn D. Burton, Nathaniel N. Urban, and Richard C. Gerkin. NeuroElectro: a window to the world’s neuron electrophysiology data. *Frontiers in Neuroinformatics*, 8:40, 2014. ISSN 1662-5196. doi: 10.3389/fninf.2014.00040. URL <http://journal.frontiersin.org/article/10.3389/fninf.2014.00040>.
- P Sanz Leon, SA Knock, M Marmaduke Woodman, L Domide, J Mersmann, AR McIntosh, and V Jirsa. The virtual brain: a simulator of primate brain network dynamics. *Frontiers in Neuroinformatics.*, 7:10, 2013. ISSN 1662-5196. URL <https://www.frontiersin.org/article/10.3389/fninf.2013.00010>.
- M.J. Brookes, J.R. Hale, J.M. Zumer, C.M. Stevenson, S.T. Francis, G.R. Barnes, J.P. Owen, P.G. Morris, and S.S. Nagarajan. Measuring functional connectivity using MEG: Methodology and comparison with fcMRI. *Neuroimage*, 56(3):1082–1104, 2011. URL <https://doi.org/10.1016/j.neuroimage.2011.02.054>.
- DW Zimmerman, BD Zumbo, and RH Williams. Bias in estimation and hypothesis testing of correlation. *Psicologica*, 24:133–158, 2003.
- Zhao Zhu, Johanna M. Zumer, Marianne E. Lowenthal, Jeff Padberg, Gregg H. Recanzone, Leah A. Krubitzer, Srikantan S. Nagarajan, and Elizabeth A.

- Disbrow. The relationship between magnetic and electrophysiological responses to complex tactile stimuli. *BMC Neuroscience*, 10(1):4, 2009. ISSN 1471-2202. URL <https://doi.org/10.1186/1471-2202-10-4>.
- G. Buzsaki, C.A. Anastassiou, and C. Koch. The origin of extracellular fields and currents - EEG, ECoG, LFP and spikes. *Nat Rev Neurosci*, 13:407–420, 2012.
- G Susi, SM Ye-Chen, J de Frutos Lucas, G Niso, and F Maestú. Neurocognitive aging and functional connectivity using magnetoencephalography. In *Oxford research encyclopedia of psychology and aging*. Oxford University press, Oxford, 2018b.
- Julien Ponge. Fork and join: Java can excel at painless parallel programming too! Oracle technology network, 2011. URL <http://www.oracle.com/technetwork/articles/java/fork-join-422606.html>.
- G. Niso, R. Bruña, E. Pereda, R. Gutiérrez, R. Bajo, F. Maestú, and F. del Pozo. HERMES: Towards an integrated toolbox to characterize functional and effective brain connectivity. *Neuroinformatics*, 11(4):405–434, 2013.
- J. Reutimann, M. Giugliano, and S. Fusi. Event-driven simulation of spiking neurons with stochastic dynamics. *Neural Computation*, 15:811–830, 2003.
- F. Naveros, J.A. Garrido, R.R. Carrillo, E. Ros, and N.R. Luque. Event- and time-driven techniques using parallel cpu-gpu co-processing for snn. *Frontiers in neuroinformatics*, 11(7), 2017.